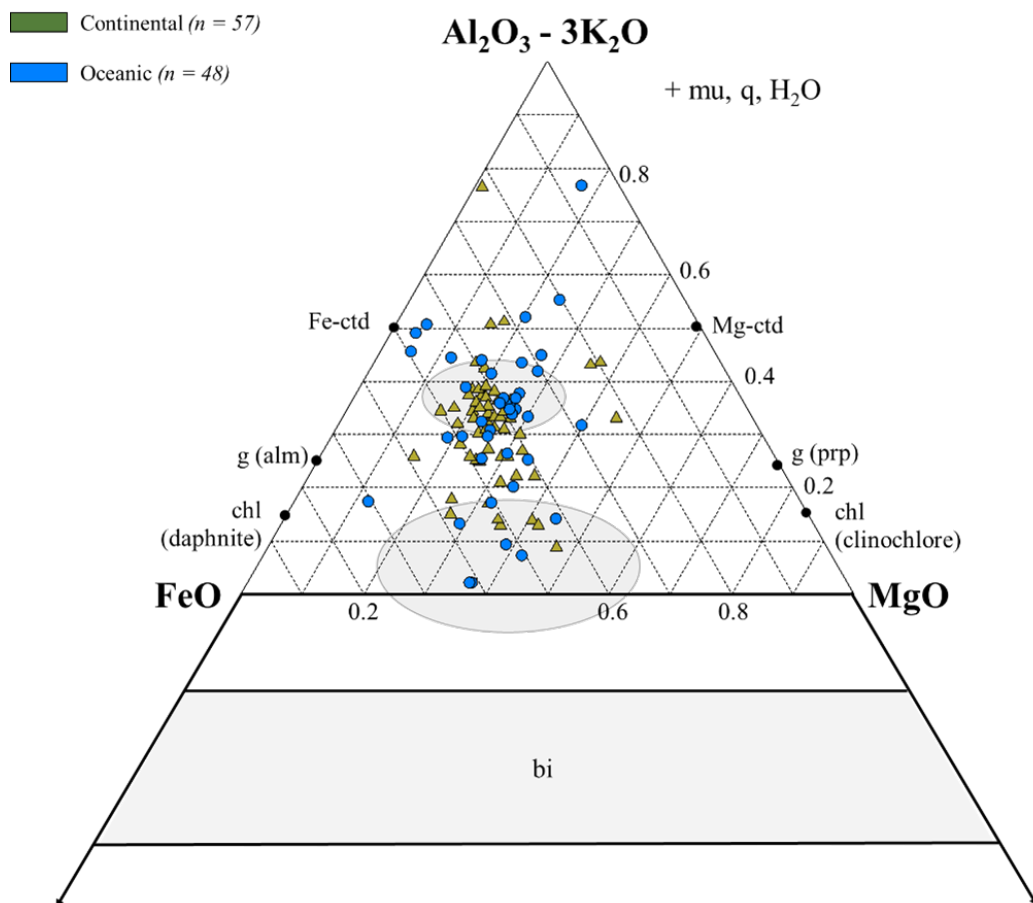




Variability of bulk rock composition of metapelites in the Alpine realm

Jenna Segerlund Henriksson



Stockholm 2025

Abstract

This study investigates the bulk rock composition of metapelites across different Alpine domains, on the basis of a literature review. Results were visualized using AFM and ACFM ternary projections to evaluate geochemical trends. Results show significant variability in bulk rock composition among different Alpine domains. Both the Adriatic and European plates host aluminous-rich metapelites which is consistent with their clay-rich continental sedimentary origin. The Valais Basin and Piemonte-Liguria Ocean domains (Lower and Upper Penninic nappes) show higher FeO+MgO concentrations which suggest oceanic sedimentation.

The median bulk composition for an Alpine metapelite calculated in this study is as follows:

SiO₂ = 57.61, TiO₂ = 0.88, Al₂O₃ = 20.50, FeO_{total} = 8.20, MnO = 0.12, MgO = 2.39, CaO = 0.58, Na₂O = 1.03, and K₂O = 3.53.

This median composition is quite similar to the median worldwide pelite recently calculated by Forshaw and Pattison (2023).

Contents

1. Introduction	1
1.1 The Alpine Realm	1
1.2 Metapelites: from sediments to metamorphic rocks	3
1.3 What is a bulk rock composition?	5
1.4 How can we measure bulk rock compositions?	5
1.5 Use of bulk rock composition in petrology	8
2. Methods	11
2.1 Literature review	11
2.2 Dataset and bulk rock chemistry	13
2.3 Ternary projections - visualizing the AFM and ACFM diagrams using Petrograph beta 2.0 (2007)	14
3. Results	16
3.1 Metapelites in the Alpine realm: a survey	16
3.2 Metapelites across the Alpine belt	17
3.3 Metapelites in the Western vs. Central vs. Eastern Alps	19
3.4 Metapelites in continental vs. oceanic domain	23
3.5 Metapelites in oceanic domains vs. European plate vs. Adriatic plate	26
3.6 Metapelites in different geological units in the Alps	31
3.7 Metapelites in the Alps and their metamorphic conditions	34
4. Discussion and conclusions	37
4.1 Bulk rock chemistry of Alpine metapelites and comparison with other belts	37
4.2 Bulk rock chemistry of metapelites across the Alpine belt	39
4.3 Bulk rock chemistry of metapelites: oceanic domain vs. Adriatic plate vs. European plate ..	39
4.4 Bulk rock chemistry of metapelites in different geological units	40
5. Future work	41
6. Acknowledgments	41
7. References	42
8. Appendix	46

1. Introduction

The Alpine region is a complex and big area of interest for many geoscientists. Known for its geological complexity, it hosts a diverse variety of rock types, including a significant presence of metapelites. The aim of this study is to discuss the variability of bulk rock composition of metapelites in the Alpine realm considering (i) palaeogeographic domain and tectonic units, (ii) their present geographical occurrence (Western, Central, and Eastern Alps), (iii) their depositional environment (i.e. continental vs. oceanic), (iv) the metamorphic grade experienced during the Alpine orogeny.

1.1 The Alpine Realm

The Alpine belt is a famous arcuate mountain range and extends over a distance of 1000 km from the Mediterranean to the Vienna basin (e.g., Pfiffner 1993). The Mont Blanc is the highest mountain (at 4888 m above sea level) of the Alpine orogen, which extends also below the surface reaching a depth of 60 km in the axial part of the belt. The Alps are geographically divided into three main domains (Figure 1):

- 1) The Western Alps, which extends from the Mediterranean coast to the Simplon Fault.
- 2) The Central Alps, which extends from the Simplon Fault to the Engadine Window.
- 3) The Eastern Alps, which extends from the Engadine Window to Vienna.

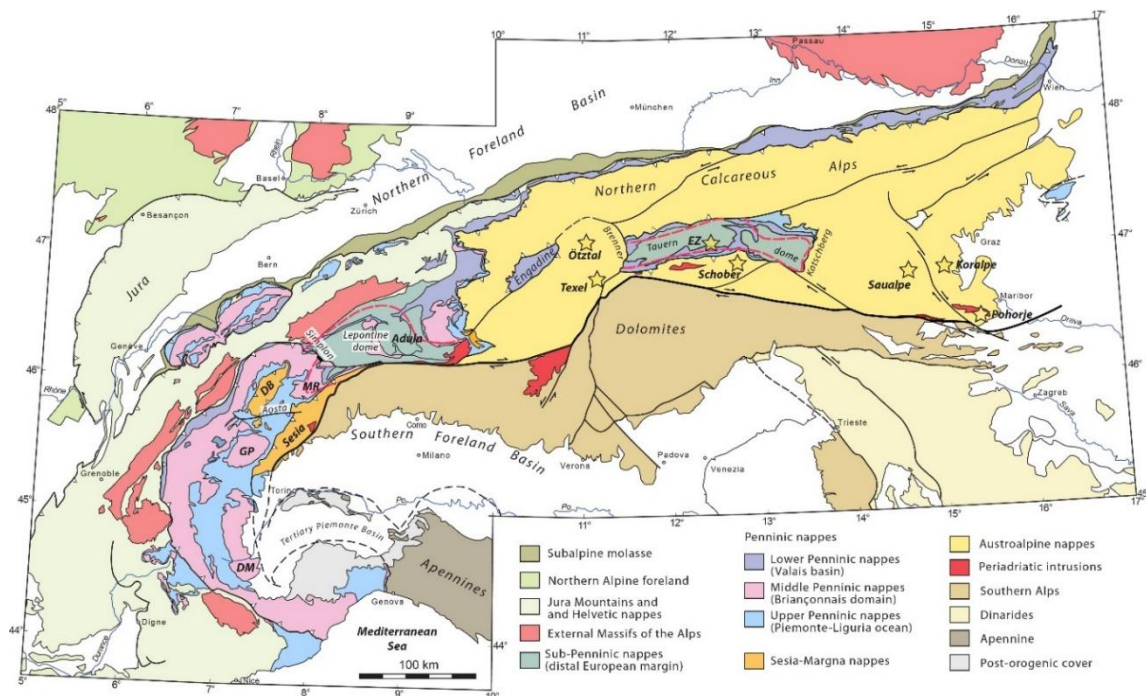


Figure 1. Tectonic map of the Alps displaying the main geological domains (Manzotti and Ballèvre, 2024).

The Alps results from the collision between the European and African plates, after closure of the Jurassic Piemonte-Liguria Ocean, a process that started in the Cretaceous (e.g., Manzotti and Ballèvre 2024). The Alps consists of a stack of nappes deriving from both continental and oceanic domains. Some of these nappes have been involved in the subduction zone before the final collision. The following palaeogeographic domains can be distinguished (Figure 1, Manzotti and Ballèvre 2024):

1. The *Adriatic Palaeomargin* comprises (i) the Sesia-Dent Blance nappes in the Western Alps that experienced blueschist to eclogite-facies metamorphism during the Alpine orogeny (Figure 2) and (ii) the Austroalpine nappes that consists of unit equilibrated at eclogite (e.g., Koralpe and Pohorje) and amphibolite-facies conditions (e.g., Rappold Complex). (iii) The Southern Alps (Figure 1) are also part of the Adria plate; they represent the upper plate and they were not involved in the Alpine cycle. The Ivrea Zone belongs to the Southern Alps and hosts metapelites that recorded pre-Alpine (Permian) amphibolite to granulite-facies metamorphism.
2. The *Penninic nappes* comprises remnants of the Piemonte-Liguria Ocean (Upper Penninic nappes, Figure 1) and Valais Basin (Lower Penninic nappes). They record blueschist- and eclogite-facies metamorphism (Figure 2). The Briançonnais domain belong to the Middle Penninic nappes, it is interpreted as a microcontinent derived from the European palaeomargin and experienced Alpine eclogite-facies metamorphism (Figure 2).
3. The *Sub-Penninic nappes* represent the distal European margin. In this domain, the Adula nappe and the Tauern Window (Eclogite Zone) preserve eclogite-facies metamorphism.

1.2 *Metapelites: from sediments to metamorphic rocks*

Metapelites is one of the most common types of metamorphic rock, derived from the metamorphism of fine-grained sedimentary rocks essentially made of clay (<4 µm) and silt (4–62 µm) size grains. Typical examples are mudrock (non fissile) and shale (fissile, Klein and Philpotts 2017). From a geochemical perspective, metapelites display high Al₂O₃ and K₂O and low CaO contents, that reflect the high modal amount of clay minerals (e.g., kaolinite, smectite, montmorillonite) and micas (e.g., detrital or authigenic muscovite, paragonite) in the original sediment (Winter 2014).

During burial and diagenesis, mud rock and shale undergo drastic chemical and mechanical changes. Their high porosity gradually decreases due to compaction and H₂O expulsion. This process also leads to the development of the characteristic slaty cleavage as a consequence of the reorientation of sheet silicates. With increasing metamorphic grade, shales transform into slate and phyllite.

Metapelites are sensitive to variations in pressure (P) and temperature (T) conditions: characteristic mineral assemblages form during progressive metamorphism (i.e., at increasing P and T conditions). When metamorphism begins, clay minerals (e.g., smectite) are replaced by chlorite and illite. In addition, carbonaceous matter may be converted into graphite or escapes as CO₂ or CH₄ together with water. Throughout the majority of metamorphic grade, metapelites contain quartz and muscovite.

George Barrow (1893, 1912) was the first to explore the variation in rock types and mineral assemblages with progressive metamorphism. He found systematic mineralogical changes in pelitic rocks at increasing T conditions and subdivided the area of study into a series of metamorphic zones, based on the appearance of a new index mineral:

- *Chlorite zone*
- *Biotite zone*
- *Garnet zone*
- *Staurolite zone*
- *Kyanite zone*
- *Sillimanite zone*

For instance, when a rock crosses the biotite isograd, it enters the biotite zone. However, it is today evident that in rocks from the same grade, a mineral can occur in some pelites and not in other ones depending on the bulk rock compositions. Bulk rock composition is therefore a key variable and it may affect the grade at which a specific mineral first appears or whether it appears or not at all.

In the Alps, the metamorphic conditions (including both P and T) increase from the external zone to the internal zone (Figure 2, Tajčmanova et al. 2021; Manzotti and Ballèvre 2024). Specifically, a sequence of minerals has been described at increasing metamorphic conditions:

- At P-T conditions of 300-400 °C and ~1.5-2.5 GPa, carpholite (lowest T) then chloritoid (higher T) developed, as observed in Mesozoic metasediments of units of continental origin.
- In the Monte Rosa, Gran Paradiso, and Dora-Maira Massifs, at P-T conditions of 450-550 °C and ~1.5-2.5 GPa, garnet-chloritoid and talc grew in Fe-rich and Mg-rich metapelite, respectively.
- At P-T conditions of ~550-600 °C and ~2.0-2.5 GPa, garnet-chloritoid-kyanite formed as observed for example in the Sesia zone and Tauern Window.
- At P-T conditions of ~730-790 °C and ~3.7-4.3 GPa, garnet-kyanite, garnet-talc-kyanite or talc-kyanite assemblages formed as described in the Brossasco-Isasca Unit. The high P-T conditions are also recorded by coesite inclusions in garnet.

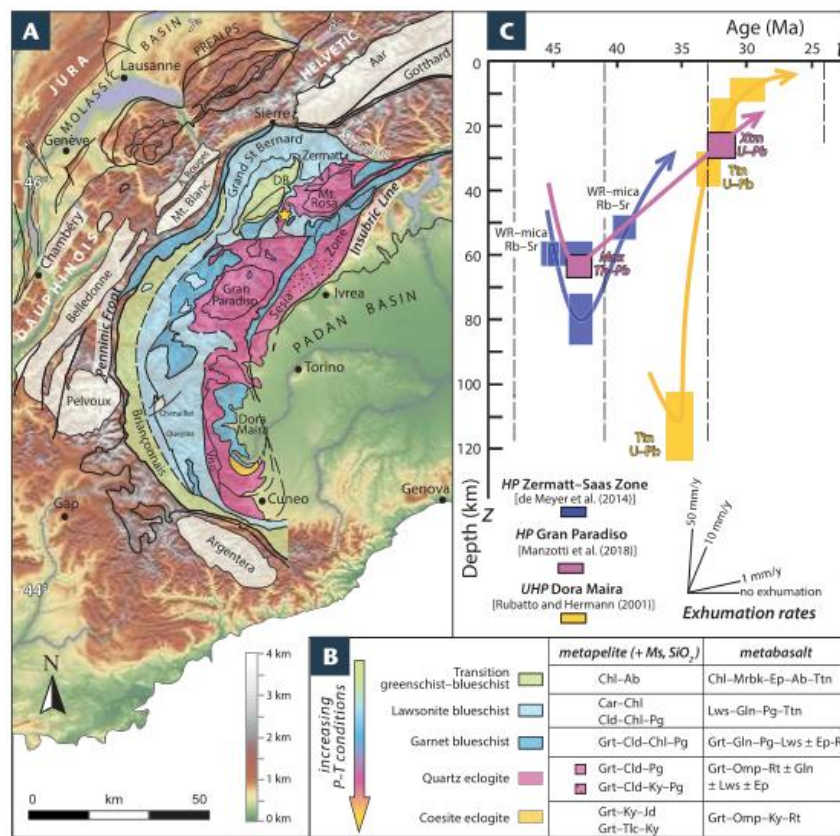


Figure 2. (A) Metamorphic map of the Western Alps. (B) Diagnostic mineral assemblages as a function of metamorphic facies in the two reference lithologies of metapelite and metabasalt, mineral abbreviations are: Ab = albite; Car = carpholite; Chl = chlorite; Cld = chloritoid; Ep = epidote; Gln = glaucophane; Grt = garnet; Jd = jadeite; Ky = kyanite; Lws = lawsonite; Mrbk = magnesioriebeckite; Rt = rutile; Tlc = talc; Ttn = titanite. (C) Burial and exhumation rates for main locations in oceanic and continental units (Tajčmanova et al. 2021).

1.3 *What is a bulk rock composition?*

To start off, we will delve deeper into how bulk rock composition is defined. The overall composition of a rock can be expressed by quantitative geochemical analysis, which comprises the percentage by mass of each of the main chemical constituents (Winter 2014). The latter are divided between major (>1.0 wt. %), minor (0.01-1.0 wt. %) and trace elements (<0.1 wt. %). Major elements are: SiO₂, Al₂O₃, FeO, MgO, CaO, Na₂O, and K₂O, and common minor elements are TiO₂, MnO, P₂O₅, the volatiles H₂O and CO₂ may also be included in this category. The major element composition of a rock influence properties such as density, diffusivity, and viscosity.

1.4 *How can we measure bulk rock compositions?*

The bulk rock composition of a rock can be measured by quantitative analysis, which measures the concentrations of major, minor and trace constituents. Bulk or ‘whole-rock’ analyses are designed to measure the holistic makeup of a homogenous sample like a rock powder. Certain applications require analysis of material that is available only in small quantities, or which is only one of several materials present in a mixed sample (e.g., analyzing specific crystals of a mineral *in situ* in a rock section), or the task may be mapping the distribution of one element in a heterogenous material (Gill 1997). In these situations, one must use a technique with spatially resolved analysis capability, like electron probe microanalysis or laser-based methods. This project focuses on the three following geochemical analytical methods:

- X-ray fluorescence (**XRF**).
- Scanning electron microscopy (**SEM**).
- Point counting.

These methods are characterized by advantages and disadvantages as detailed below and display different accuracy and precision. Accuracy describes how close results are to the true value, while precision describes the reproducibility of a technique with arbitrary distributed errors (Winter 2014).

Method A: XRF (X-ray fluorescence)

An X-ray fluorescence (XRF) analysis is a method that is typically used for measuring bulk rock compositions through specially prepared solids or powders. The XRF irradiates a solid sample with X-rays that are sufficiently energetic in order to then excite the electron transitions in the inner electron shells for an array of different elements in a single properly prepared sample. The subsequent return to the ground state will result in a discharge of fluorescent X-rays of the unique spectra in the higher-energy X-ray range. This entire process is mainly controlled by a computer that also performs and reports data reduction and gauges the concentrations of the elements into specialized software. According to studies conducted by Ramsey et al. (1995) the precision for major elements (e.g. TiO₂, SiO₂ and MgO) by fusion for XRF is 0.23%, whereas the precision value for trace elements is 1.5% (including Rb and Th).

Method B: area-scan method at SEM-EDS

In contrast to XRF analysis, the area-scan method uses a scanning electron microscope (SEM) (Figure 3). The instrument analyzes the sample by bombarding a polished thin section of the specimen with a beam of electrons, similarly to XRF, whereas the result is the emission of X-rays which are characteristic to the presence of the particular inorganic elements in the sample. The SEM-EDS method has a detection limit of 0.1 wt.% (e.g., Kuisma-Kursula 2000). However, Kuisma-Kursula's experiments show that the accuracy and precision of measurements regarding Na by SEM-EDS had a range of 10-30%. This is due to the concentration of Na being under 1 wt.% in the analyzed lead glass and therefore close to the detection limit for EDS method.

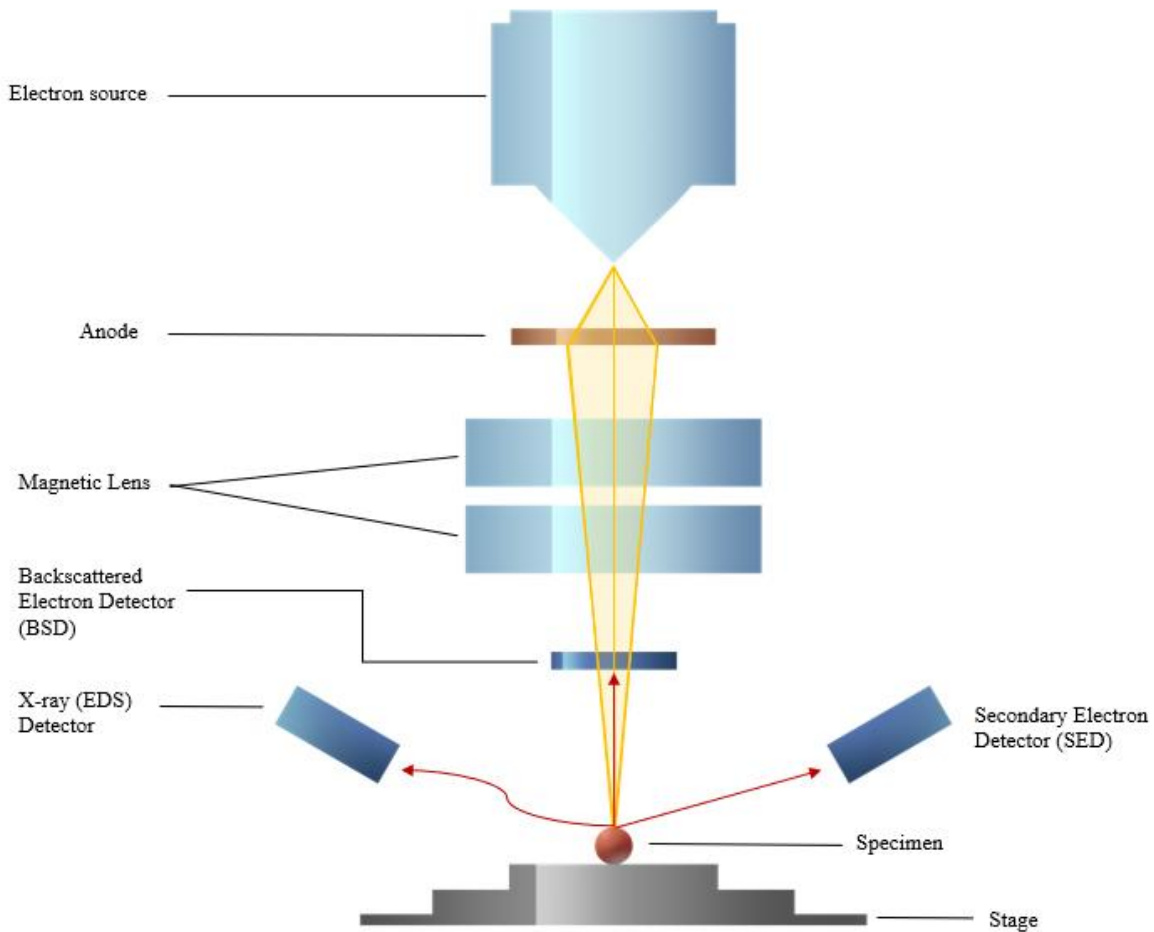


Figure 3. Image of a SEM instrument with EDS and SED attachments respectively, illustration made by me.

Method C: Modal proportions and chemical compositions of the mineral present

The bulk rock composition can also be measured by combining point counting (modal proportions) with the chemical compositions of the minerals present in a rock (method C). The determination of modal proportions through point counting is commonly done using a mechanical apparatus (Figure 4) that moves the section along a two-dimensional grid on the petrographic microscope stage, with each shift the mineral at the crosshair of the telescope is to be identified and then counted. The total amount of points counted (usually several hundred), the count for each mineral is then summed and totals are normalized to 100% to determine the final modal proportion.

Ross (2021) notes that the “point counting” method only determines specific areas of the minerals, but the result tend to have a direct relationship with the total volume of the studied rock, i.e. even if there are for example individual variations, these properties typically scale with the overall size of the rock. The point counting method in modal analysis can vary in terms of accuracy and precision alike (Ross 2021). In order to reach a high precision in this method, it is vital to conduct a sufficiently high number of counts, contemporary error charts, in contrast to older ones, incorporate key factors like voids, matrix and cement which has helped to increase the overall precision of the method. The challenge of maintaining precision is based on the component with the least abundance, which requires a more strategic approach where the number of points counted is based entirely on the least abundant component of interest.



Figure 4. Example of a point counting microscope, image from CRAIC Technologies.

1.5 Use of bulk rock composition in petrology

The different roles played by the major and trace elements can each provide distinct insights into a variety of igneous processes. For instance, major elements can be used to classify igneous rocks and further give valuable insights and information regarding the role of geochemistry in the physical properties of crystal-melt systems. The trace elements may also be used to study the evolution of melts and minerals during either the crystallization or melting process. In addition, the concentration and distribution of trace elements can also be used as an effective asset to study the evolution of magmas, the possible magma source environments and/or to distinguish different magmatic processes that may have occurred during magma's evolution.

In metamorphic petrology, the bulk rock compositions are used for constructing P-T diagrams – pseudosections through equilibrium thermodynamic modelling. Pseudosections are diagrams built for a specific bulk rock composition and show the stability fields of specific mineral assemblages (e.g., Winter 2014). They also provide information on the composition of minerals stable at specific P-T conditions and their modal amounts (e.g., Zou et al. 2022). These diagrams are very useful to reconstruct the P-T conditions and evolution of metamorphic rocks and thus to decipher the orogenic history (burial and exhumation) of mountain belts.

In metamorphic petrology, bulk rock compositions are also commonly plot in ternary projections, such as **ACFM** and **AFM** ternary plots. These diagrams are very useful because they allow establishing the minerals that should be present in a rock, allowing a comparison with petrographic observations done in thin sections.

In this study, bulk rock compositions are plotted in the ternary projections ACFM and AFM. However, these diagrams are used not for establishing mineral assemblages, but to explore the geochemical variability (for major elements) of metapelites in a mountain belt (i.e. the Alps).

ACFM

The ACFM (also known as ACF, Figure 5) is a common ternary diagram within metamorphic petrology that was first used by Eskola (1915) in his studies of metamorphic rocks (Nelson 2011). Eskola's goal was to propose a diagram as a way to illustrate metamorphic mineral assemblages on a simplified ternary plot consisting of three components and only focused on minerals that appeared or disappeared during metamorphism and would therefore act as a measurement of the metamorphic grade of the rock (Winter 2014).

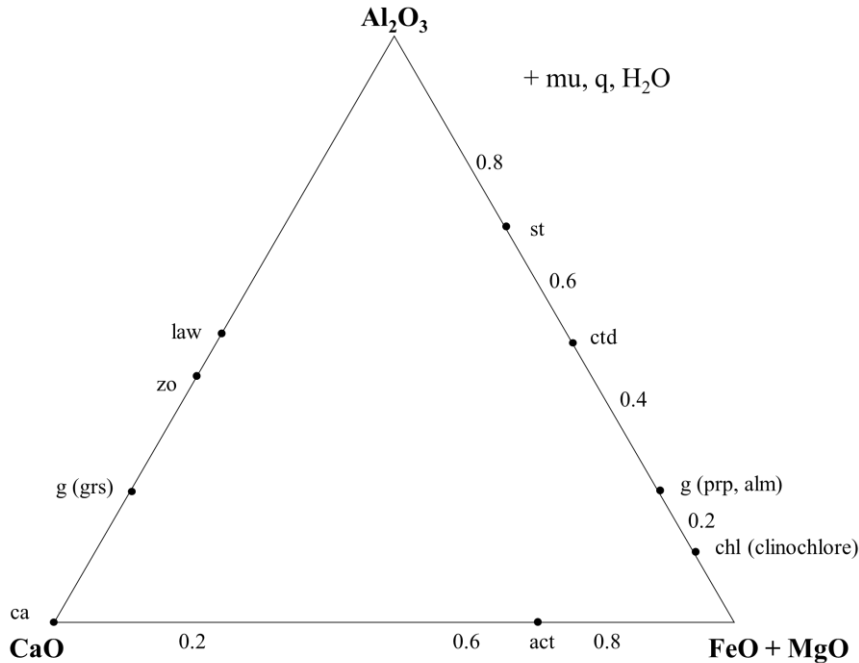


Figure 5. ACFM diagram.

To plot a rock on this diagram the geochemical data of the rock (i.e., bulk rock composition) has to be recalculated on an anhydrous basis. Then the molecular proportions are calculated by dividing the molecular weight of each oxide constituent by the molecular weight of that oxide. In these diagrams, quartz and H_2O are considered in excess.

In K-feldspar is present (Kfs), A represents the value of excess Al_2O_3 left after giving Na_2O and K_2O to form alkali feldspar.

C represents the CaO after allotting P_2O_5 to form apatite, with the assumption that any P_2O_5 in the rock will suck up CaO to form apatite" (Nelson 2011).

$$C = \text{CaO}$$

FM represents the sum of FeO and MgO

$$\text{FM} = \text{FeO} + \text{MgO}$$

AFM

The ACFM diagrams (Figure 6) are fairly simple and useful, but points out the problem that Fe and Mg are assumed to substitute for each other and together act as a single component, when minerals in natural environments with the composition of Fe – Mg solid solutions are proven to be very dependent on P-T conditions (e.g., Nelson 2011). As a result, we lose some information if we treat Fe and Mg as a single constituent rather than two separate ones.

Therefore, the AKFM diagram (typically called AFM diagram) was first proposed by J. B Thompson (1957) and is especially useful for studying metapelites. Metapelites are not only sensitive to P and T variations, but their mineralogy can change as a function of variation in their compositions (especially with respect to Fe and Mg). Therefore, it was seen as almost a necessity to propose a diagram which could display the variation in the Mg/(Mg+Fe) ratio.

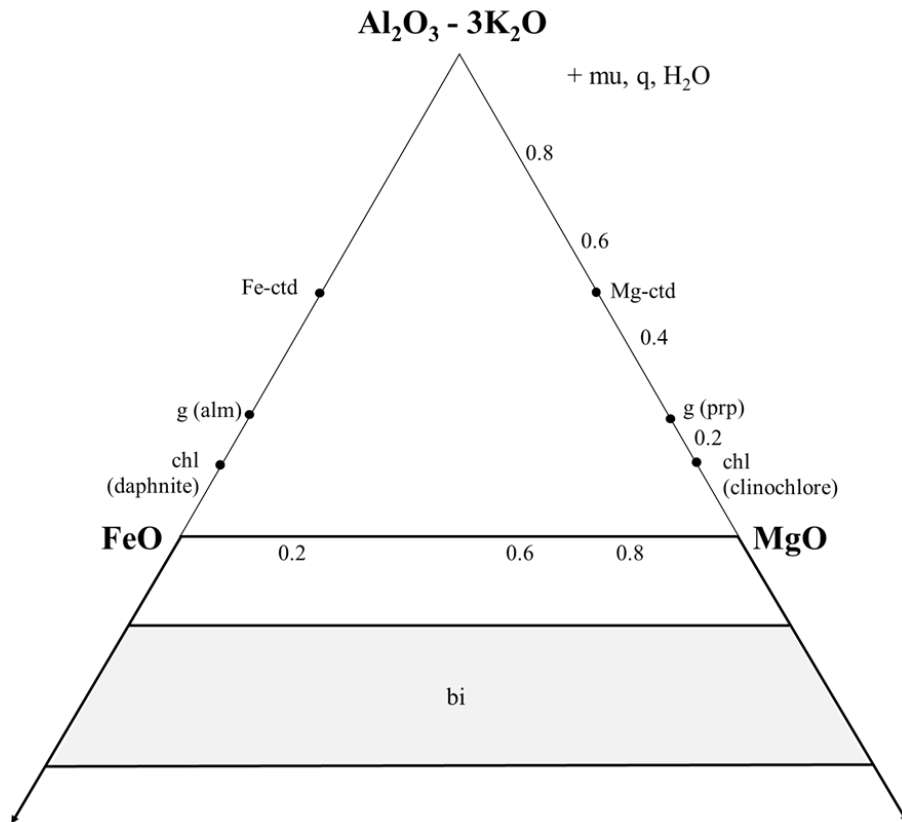


Figure 6. AFM diagram.

The AFM projection is also projected from muscovite and follows these formulas (Winter 2014):

$$A = \text{Al}_2\text{O}_3 - 3\text{K}_2\text{O} \text{ (projected from muscovite)}$$

$$F = \text{FeO}$$

$$M = \text{MgO}$$

2. Methods

2.1 Literature review

Literature review encompassed 30 written works, including journal articles and books (Figure 7 and Table 1). The reviewed literature showed a bias towards the Western Alps (e.g., Gran Paradiso, Dora-Maira, Ivrea Zone, Schistes Lustrés and Bündneschiefer zone) (Figure 8), whereas a few studies focused on metapelites from the Central (e.g., Alpe Sponda) and Eastern Alps (Pohorje Mountains, Ulten Zone and the Koralm Complex). Reporting the data was aided by an extensive dataset in the form of a Microsoft Excel Worksheet.

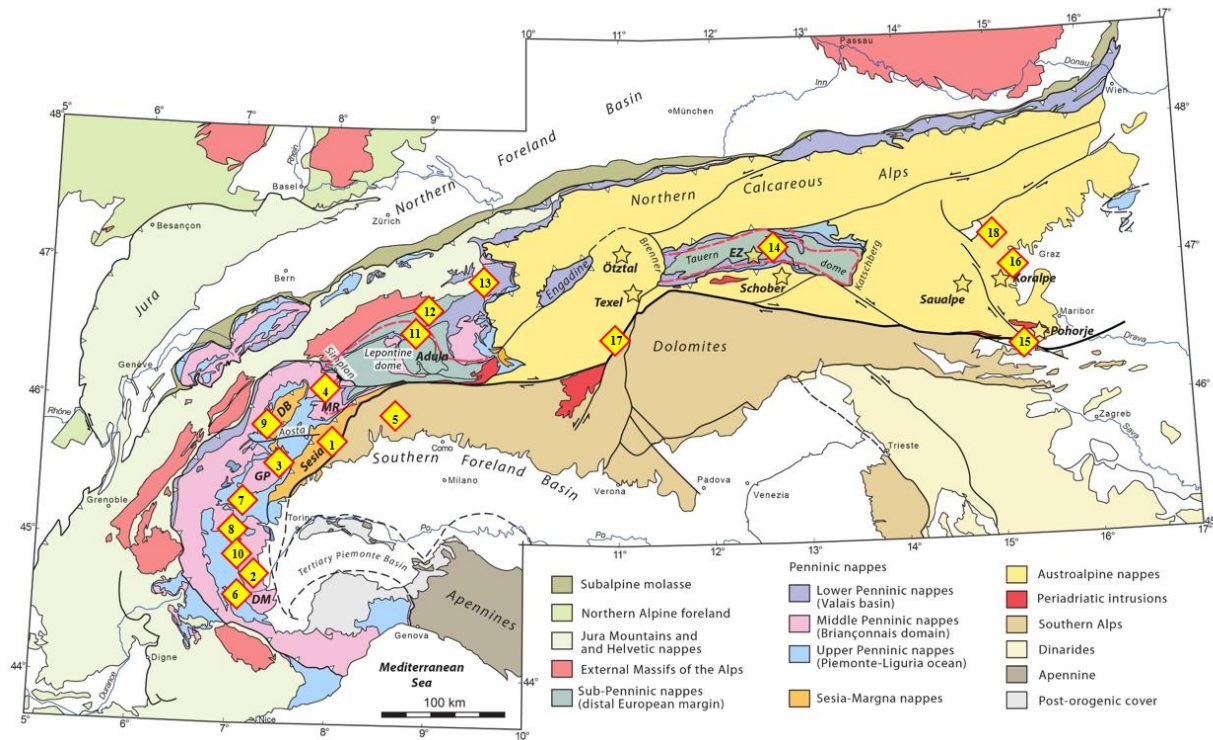


Figure 7. Map showing sample locations throughout the Alpine realm (the reference to the numbers can be found in Table 1).

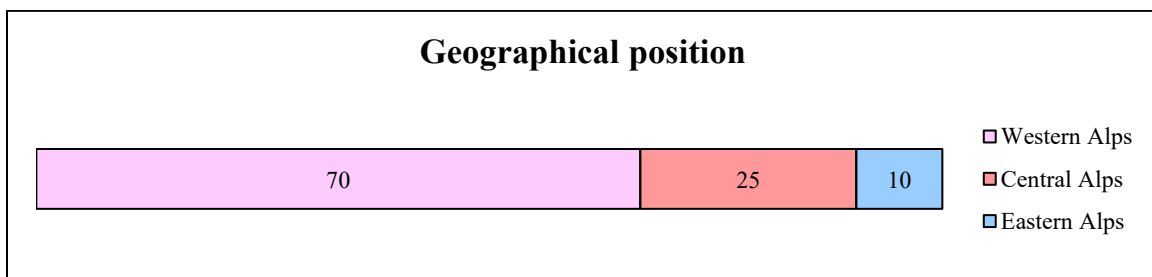


Figure 8. Chart showing the distribution of metapelites according to their geographical position, dominated by samples from the Western Alps (n=70).

GEOGRAPHIC DOMAIN	UNIT	REFERENCES
<i>Western Alps</i>		
1	Sesia Zone	Regis et al. 2014
2	Dora-Maira Massif	Groppo et al. 2019
		Manzotti et al. 2022
		Nosenzo et al. 2023
		Groppo et al. 2025
3	Gran Paradiso Massif	Le Bayon et al. 2006
		Manzotti et al. 2018
4	Monte Rosa	Keller et al. 2004
5	Ivrea Zone	Redler et al. 2012
		Wyatt et al. 2022
6	Lago Superiore Viso	Angiboust et al. 2012
 		
7	Corsica	Vitale et al. 2014
	Fraiteve	Epstein et al. 2019
8	Assietta	Epstein et al. 2019
	Queyras	Bebout et al. 2013
	Schiste Lustrés	Henry et al. 1996 Agard et al. 1999
9	Combin Zone	Manzotti et al. 2021
10	Viso Unit Piemonte	Ghignone et al. 2023
<i>Central Alps</i>		
11	Campolungo	Gieré et al. 2011
	Alpe Sponda	Redler et al. 2016
12	Brig CA	Garofalo 2012
	Passugg CA	Garofalo 2012
	Quartenschiefer & Bündnerschiefer	Janots et al. 2008
13	Bündnerschiefer	Miron et al. 2013
14	Eclogite Zone – Tauern Window	Hoschek et al. 2010
		Smye et al. 2010
<i>Eastern Alps</i>		
15	Pohorje Mountains	Li et al. 2021
		Hurai et al. 2010
16	Koraln Complex	Stüwe and Powell 1995
17	Ulten Zone	Braga and Massonne 2012
18	Wölz & Rappold Complex	Gaidies et al. 2006

Table 1. References for numbers reported in Figure 8. Vitale et al. (2014) is a study on metapelites from Corsica and thus is not reported in Figure 8.

2.2 Dataset and bulk rock chemistry

The compiled dataset categorizes 127 samples on the basis of the unit to which they belong. For each sample, (i) the mineral assemblage, (ii) the metamorphic conditions (P [GPa] and T [°C]), and (iii) the bulk rock composition are reported. For some samples (22 out of 127), some of the above information was missing. Bulk rock compositions of samples with incomplete information were not used in this study. In total, the bulk rock compositions of 105 samples out of 127 were used to build the AFM and ACFM projections both projected from muscovite and considering quartz and H₂O in excess. All iron was considered to be FeO.

Four different methods were used to measure the bulk rock composition (Figure 9):

- XRF
- Point counting
- SEM-EDS
- SEM-EDS + Point counting

In most cases (i.e., 66 out of 105 studies), the bulk rock composition was measured by XRF method (Figure 9).

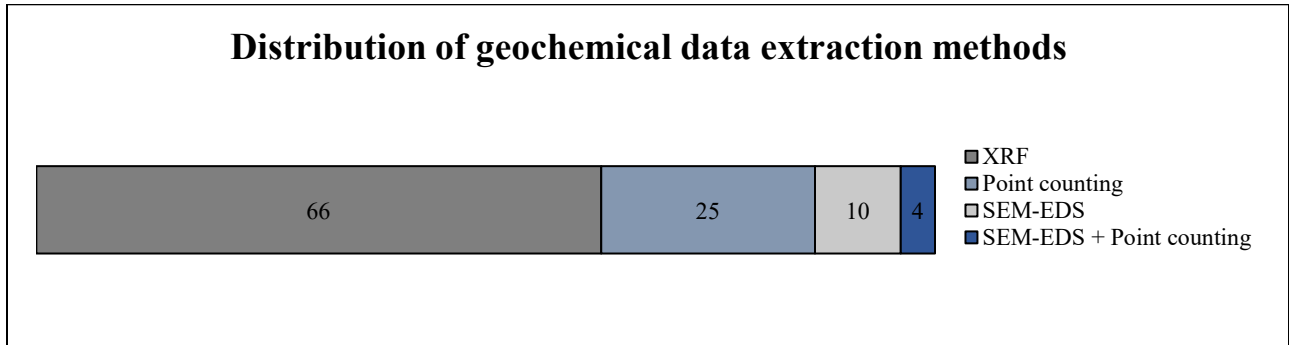


Figure 9. Staple diagram displaying the distribution of data extraction methods for the samples in this study.

2.3 Ternary projections - visualizing the AFM and ACFM diagrams using Petrograph beta 2.0 (2007)

The AFM and ACFM projections were built using PetroGraph 2.0 beta (2007), a free software developed to help the user visualize geochemical data. This software was developed by Petrelli et al. (2005) and is able to plot geochemical data on several different kind of diagrams, including classification and “petrotectonic” plots, however these functions were not utilized for this study. The software is equipped with basic functions such as the capability to handle large bundles of data, a variety of modeling possibilities like major element mass balance calculations to magma and melting evolution models (based on isotopic and trace element data). The simple user interface was easy to interpret and effectively plot the relevant diagrams for this study (Figure 10).

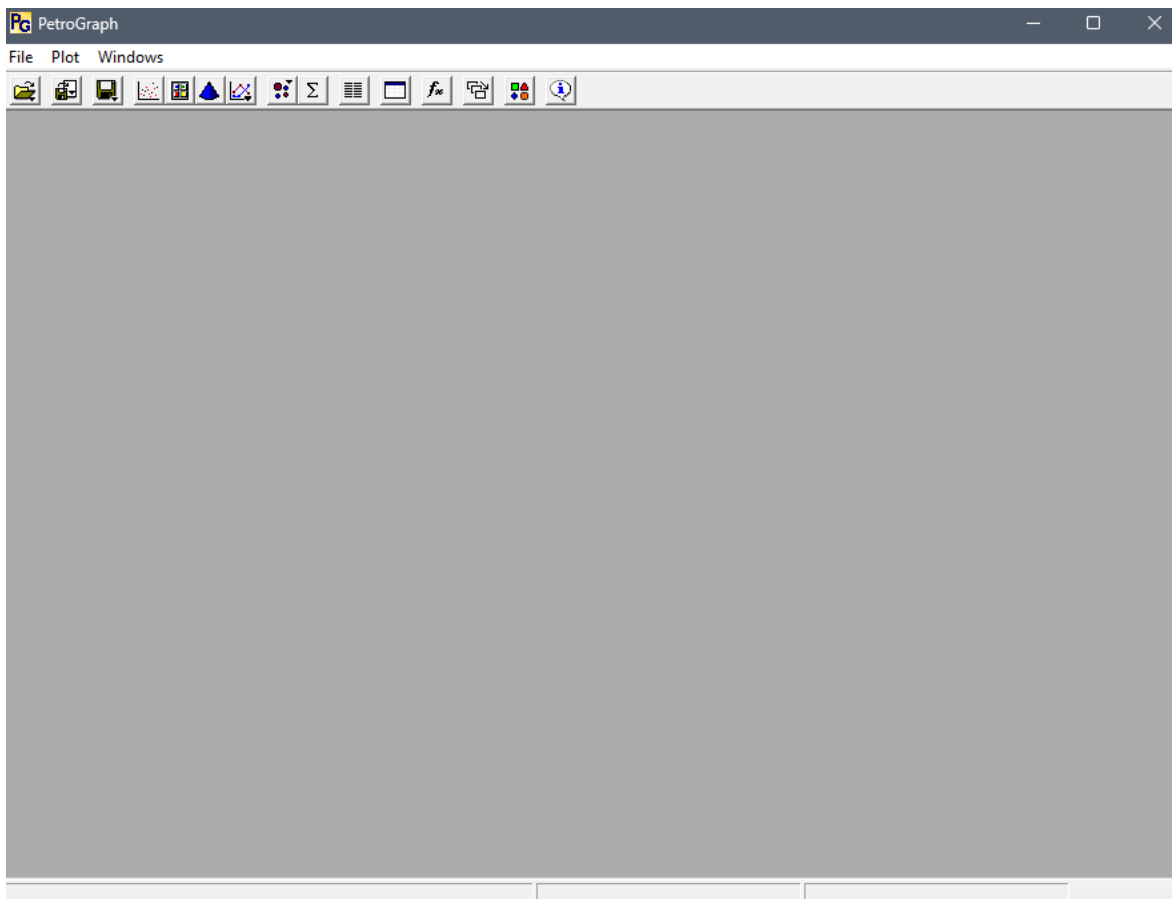


Figure 10. Home screen of PetroGraph 2.0 beta (2007).

Data input and exporting process

The data was imported into the software with Microsoft Excel Worksheet file format (.xls). The geochemical data had to be rewritten and restructured for them. This process included using a legend within the software (Figure 11) which displays symbols and colors with their corresponding numbers to be put into the .xls file to show the desired result. The data for the sample names, symbol and color were each put in three columns titled “sample”, “symbol” and “color”. The calculated coordinates for “A”, “F” and “M” and “A”, “C” and “FM” were transposed and put under their correlated columns, along with the relevant input of symbols and colors. When the prepared datafile had been successfully imported, it was ready to be plotted using three main types of diagrams in the software: binary, ternary and spider diagrams, this study exclusively used ternary projections. The ability to export either as vector graphics or in common raster formats made it possible to tweak and further modify the diagrams in other editing software such as Microsoft Excel or Clip Studio Paint.

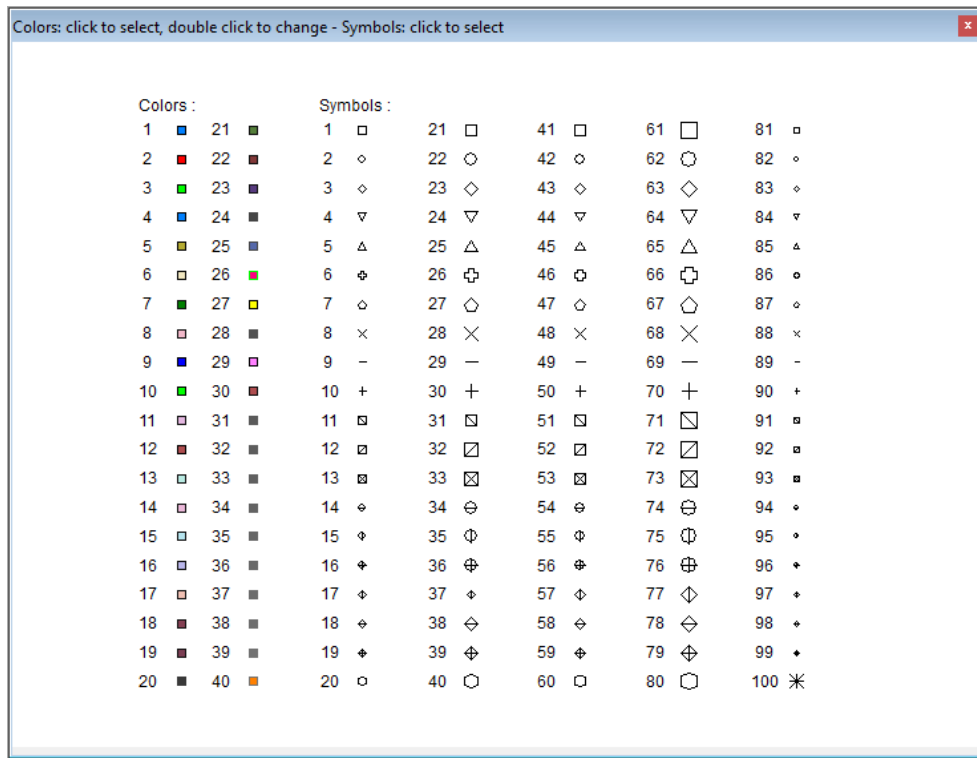


Figure 11. Color and symbol input data for PetroGraph 2.0 beta (2007).

3. Results

3.1 *Metapelites in the Alpine realm: a survey*

AFM and ACFM diagrams were built using the compiled dataset and considering muscovite, quartz and H₂O in excess. Data were first plotted together and then presented according to the following criteria:

- Geographic position
- Oceanic vs. continental affinity
- European plate vs. Adriatic plate vs. Oceanic domains
- Geological unit
- Metamorphic facies

The AFM diagrams report the fields of aluminous-rich and aluminous-poor pelites (located above or below the garnet-chlorite line, see Spear 1993). Aluminous-rich metapelites contain aluminum bearing minerals such as chloritoid, kyanite/sillimanite. These minerals do not develop in aluminous-poor metapelites.

When possible, ACFM diagrams were built distinguishing between low Ca ($C < 3$), intermediate Ca ($3 < C < 5$) and high Ca metapelite ($C > 5$). This subdivision has been recently proposed by Groppo et al. (2025). CaO-poor metapelites ($C < 3$) typically derive from pure pelites and are dominated by clays, chlorite, detrital feldspars and quartz. CaO-rich metapelites ($C > 5$) derive from calcareous pelites and contain a relatively low modal amount of carbonates (<5%).

ACFM diagrams built without this distinction as a function of geographic position and oceanic vs. continental affinity are reported in the Appendix.

In the following section, for our convenience, for each category, we first present AFM diagrams and then ACFM diagrams.

3.2 Metapelites across the Alpine belt

AFM

Most of the samples ($n = 83$) are aluminous-rich metapelites (Figure 12). The M/FM ratio ranges from 0.02 to 0.45, but most of the samples display an M/FM ratio in the range of 0.2–0.3.

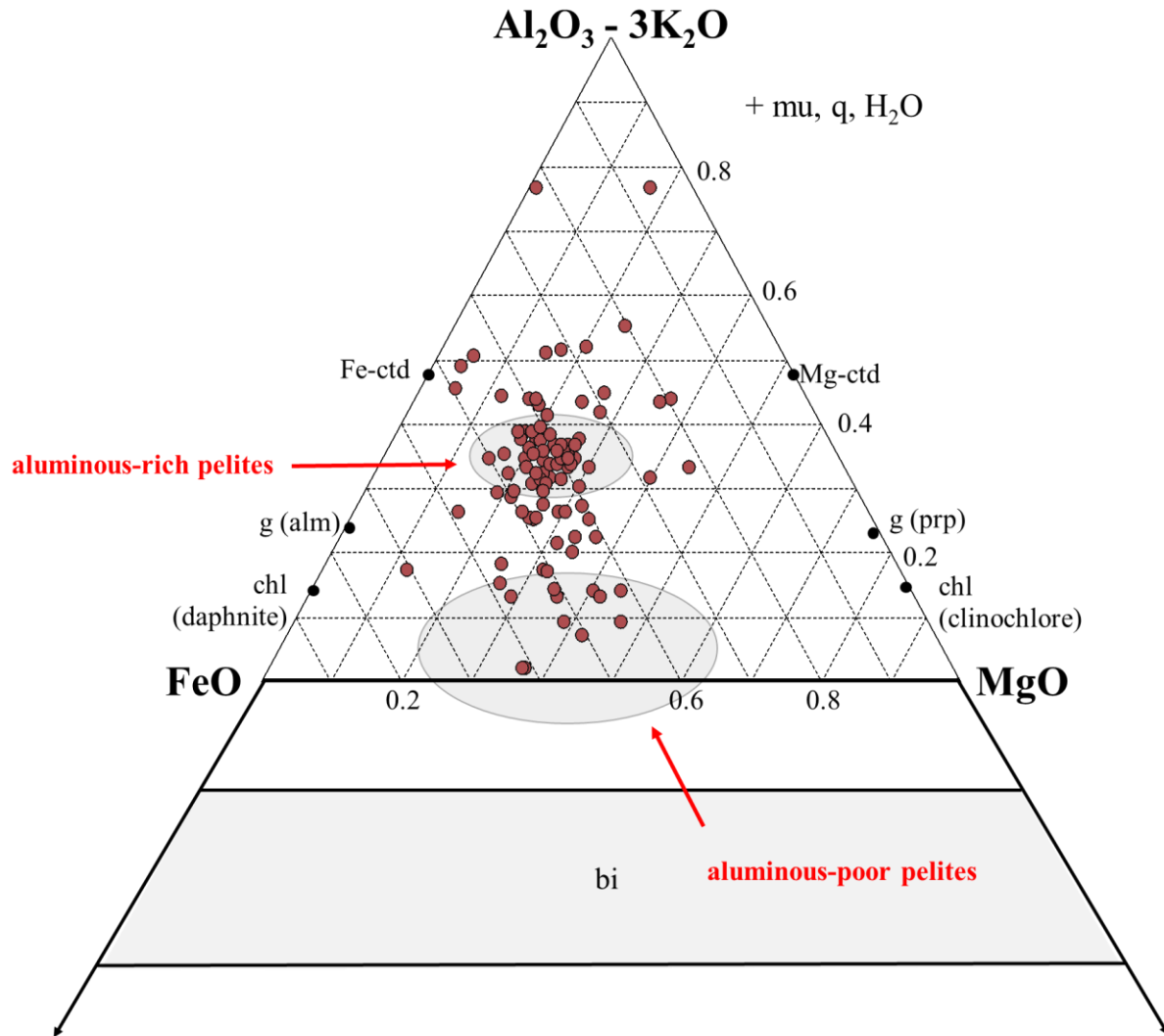


Figure 12. AFM diagram showing all samples ($n=105$) uncategorized.

ACFM

Most of the samples are low-Ca metapelites (n=48), followed by high-Ca (n=36) and intermediate-Ca (n=21) metapelites (Figure 13). The low-Ca metapelites are mainly aluminous rich ($A > 0.25$), whereas the Ca-rich metapelites display a relatively high variability in their aluminous content ($0 < A < 0.8$, Figure 14).

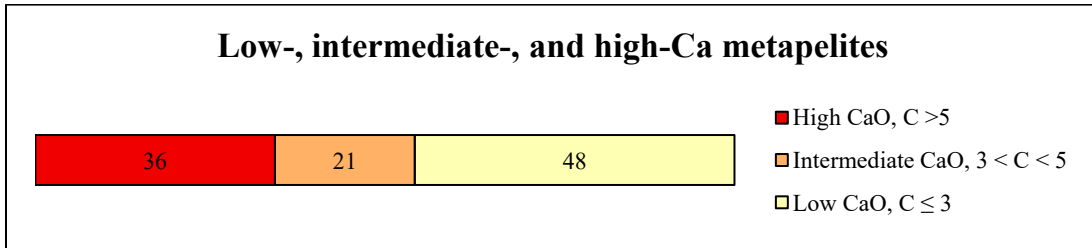


Figure 13. Chart showing the distribution of low-, intermediate- and high-Ca metapelites (n=105).

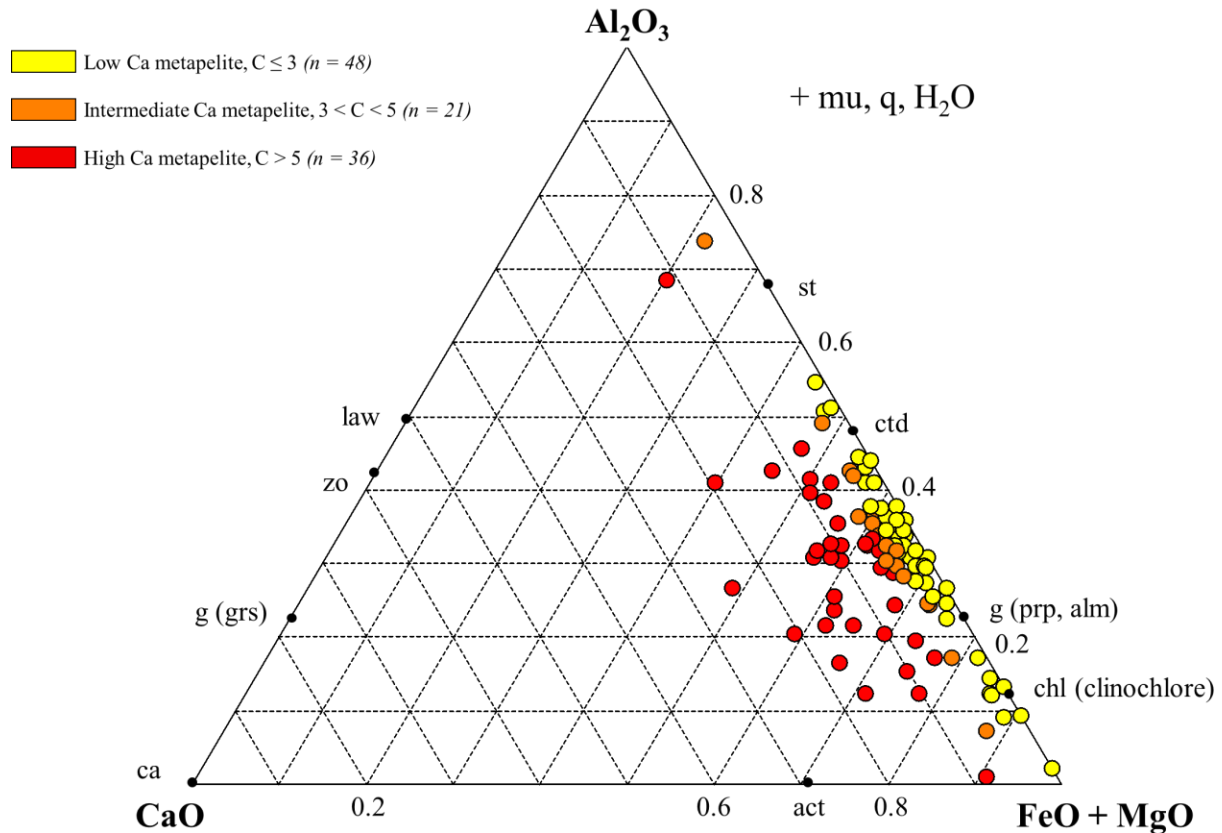


Figure 14 ACFM diagram displaying metapelites across the Alps. Data plotted using the subdivision low Ca metapelite, $C \leq 3$, intermediate Ca metapelite, $3 < C < 5$, and high Ca metapelite, $C > 5$.

3.3 Metapelites in the Western vs. Central vs. Eastern Alps

AFM

Samples from the Eastern and Central Alps are dominantly aluminous-rich metapelites ($A > 0.25$), while samples from the Western Alps comprise both aluminous-rich and aluminous-poor metapelites ($0.02 \leq A < 0.8$, Figure 15). The M/FM ratio varies between all three groups: Western Alps = 0.05–0.5, Central Alps = 0.1–0.65 and Eastern Alps = 0.15–0.32.

■ Western Alps ($n = 70$)

■ Central Alps ($n = 25$)

■ Eastern Alps ($n = 10$)

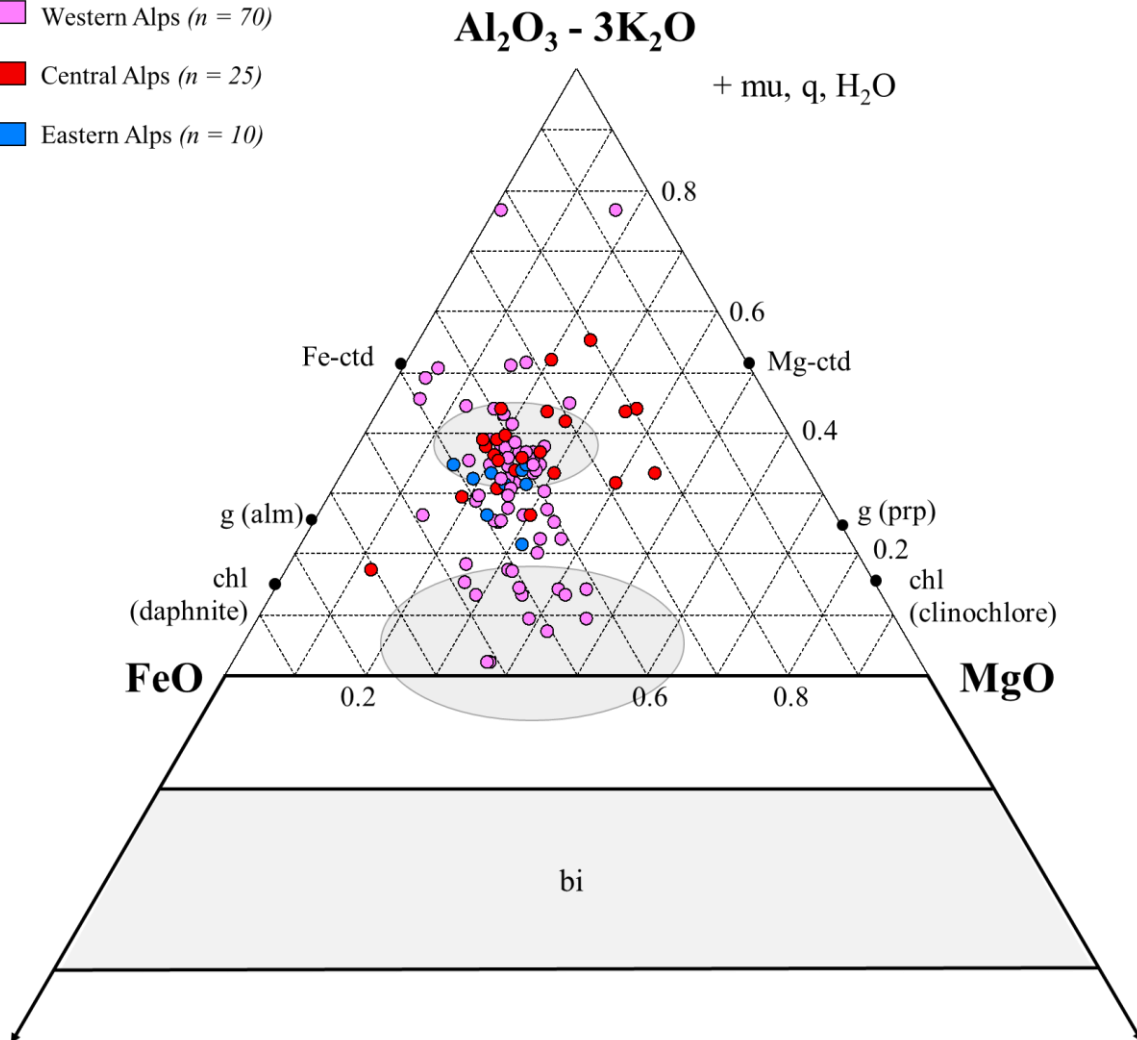


Figure 15. AFM diagram showing all ($n=105$) plotted as a function of their geographical positions (Western, Central and Eastern Alps).

ACFM

Western Alps

Most samples from the Western Alps are low-Ca metapelites ($n=27$), followed by high-Ca ($n=24$) and intermediate-Ca ($n=19$) metapelites (Figure 16). The low-Ca metapelites are mainly aluminous rich ($A>0.25$), whereas both intermediate and high Ca metapelites display a high variability in their aluminous content ($0.02<A<0.8$).

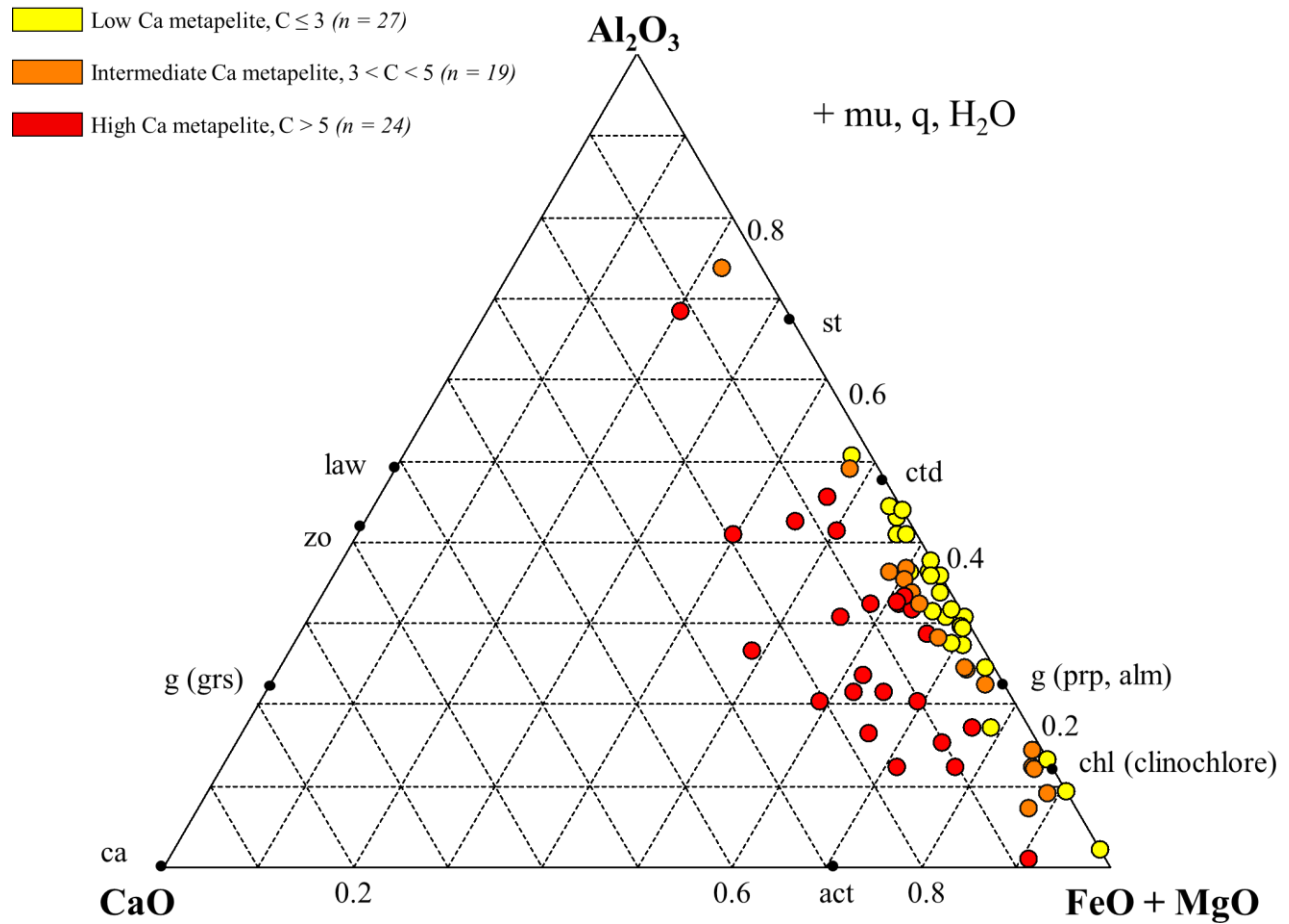


Figure 16. ACFM diagram showing all samples ($n=70$) from the Western Alps. Data plotted using the subdivision low Ca metapelite, $C \leq 3$, intermediate Ca metapelite, $3 < C < 5$, and high Ca metapelite, $C > 5$.

Central Alps

The majority of samples from the Central Alps are low-Ca metapelites ($n=13$), followed by high-Ca ($n=7$) and intermediate-Ca ($n=5$) metapelites (Figure 17). The low-Ca metapelites are mainly aluminous rich ($A>0.25$), whereas the intermediate and high Ca metapelites are all aluminous-rich with minimal variability in aluminous content ($0.25<A<0.45$).

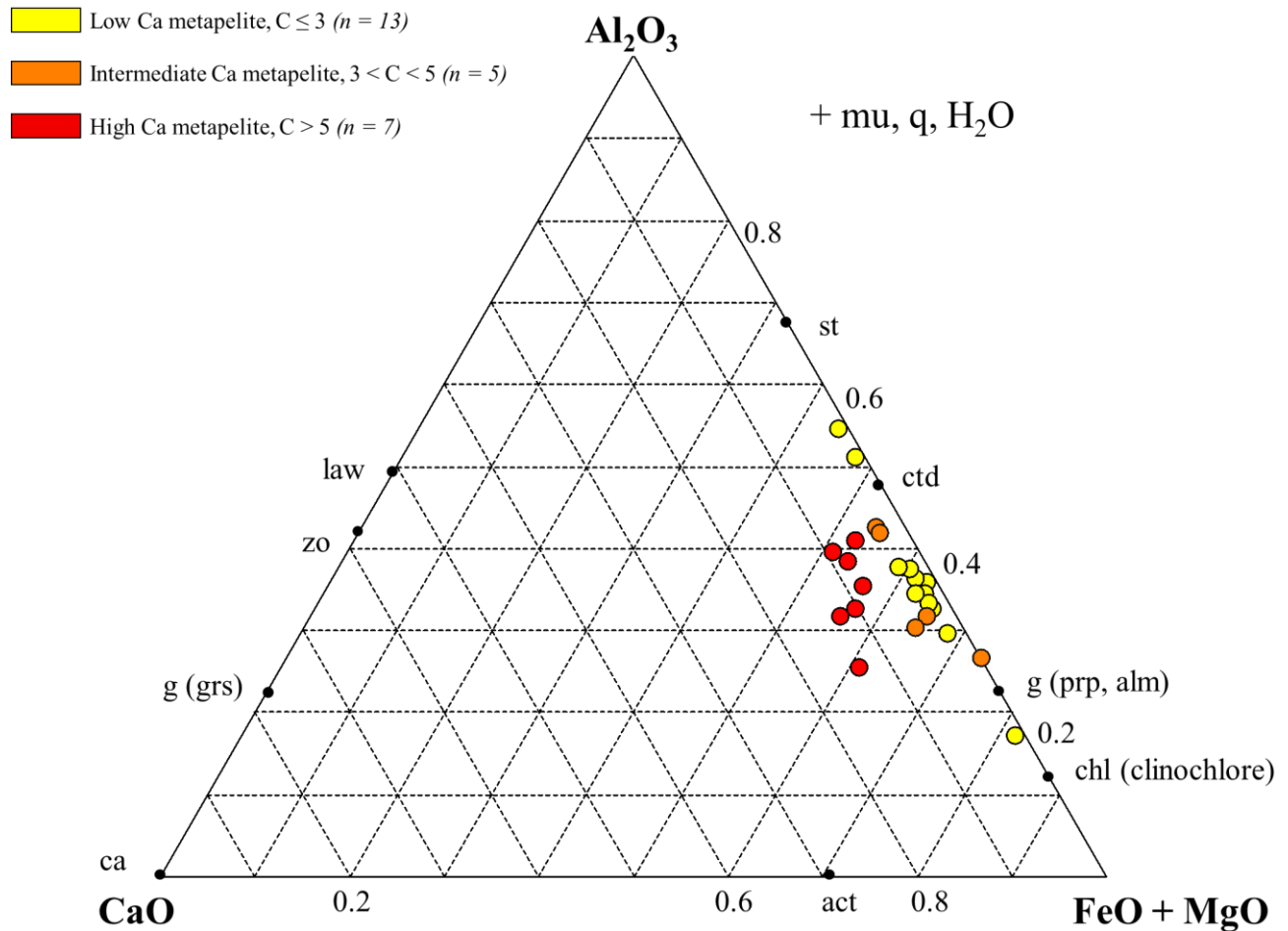


Figure 17. ACFM diagram showing all samples ($n=25$) from the Central Alps. Data plotted using the subdivision low Ca metapelite, $C \leq 3$, intermediate Ca metapelite, $3 < C < 5$, and high Ca metapelite, $C > 5$.

Eastern Alps

Most samples from the Eastern Alps are high-Ca metapelites ($n=5$), followed by low-Ca ($n=4$) and intermediate-Ca ($n=1$) metapelites (Figure 18). The low-Ca metapelites are aluminous rich ($A>0.25$), whereas the high-Ca metapelites display some variability in their aluminous content ($0.2\leq A<0.35$). The only intermediate Ca metapelite is aluminous-rich ($A>0.25$).

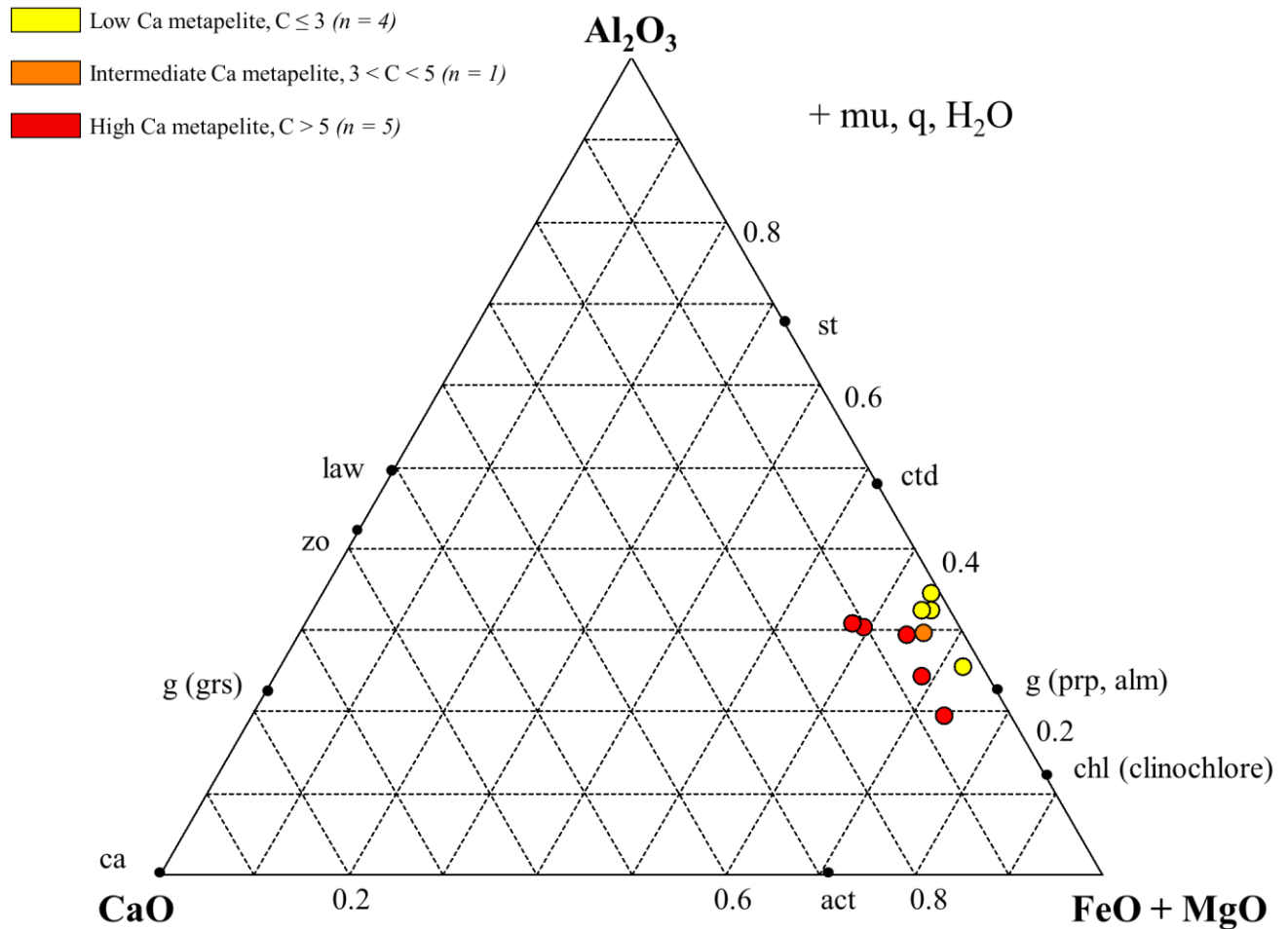


Figure 18. ACFM diagram showing all samples ($n=10$) from the Eastern Alps. Data plotted using the subdivision low Ca metapelite, $C \leq 3$, intermediate Ca metapelite, $3 < C < 5$, and high Ca metapelite, $C > 5$.

3.4 Metapelites in continental vs. oceanic domain

The majority of samples belong to continental domain (n=57), but samples from oceanic domain are also well represented (n=48) (Figure 19). The continental and oceanic metapelites are mainly aluminous-rich. The M/FM ratio of samples from the continental and oceanic domains range from 0.02 to 0.6 and 0.05–0.45, respectively (Figure 20). However, most samples from continental domain display a relatively narrow M/FM ratio, comprised between 0.35 and 0.45. By contrast, data from the oceanic domain are more dispersed. Metapelites from oceanic domain display higher MgO (up to 71 mol%) and FeO (up to 63 mol%) compared to the ones from the continental domain.

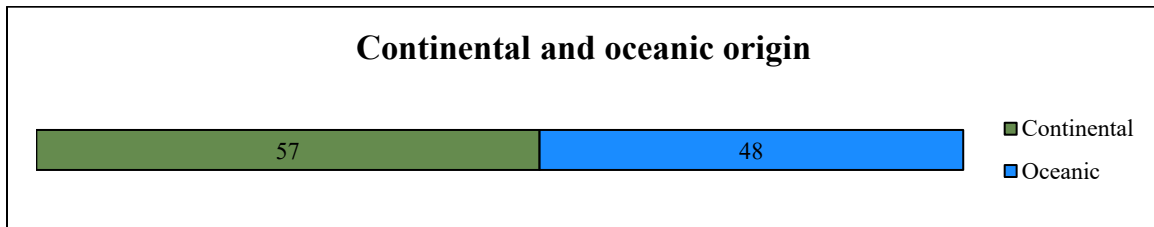


Figure 19. Chart showing the distribution of metapelites of continental and oceanic origin/remnant between all samples (n=105).

AFM

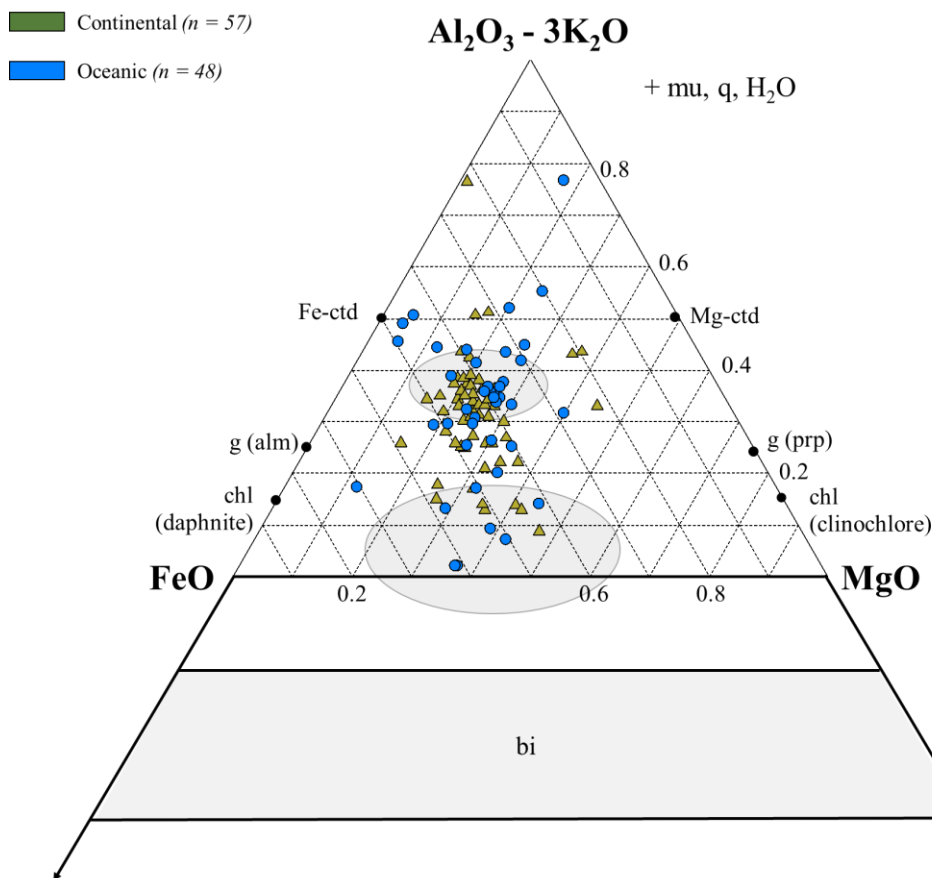


Figure 20. AFM diagram showing all samples (n=105) plotted as a function of their affinity (continental vs. oceanic).

ACFM

Continental domain

Most samples are low-Ca metapelites ($n=29$), followed by high-Ca ($n=17$) and intermediate-Ca ($n=11$) metapelites (Figure 21). The intermediate-Ca metapelites are mainly aluminous-rich ($A>0.25$), whereas low Ca metapelites ($0.1\leq A<0.6$) and high Ca metapelites ($0.1<A<0.7$) show variability in concentrations of aluminous minerals.

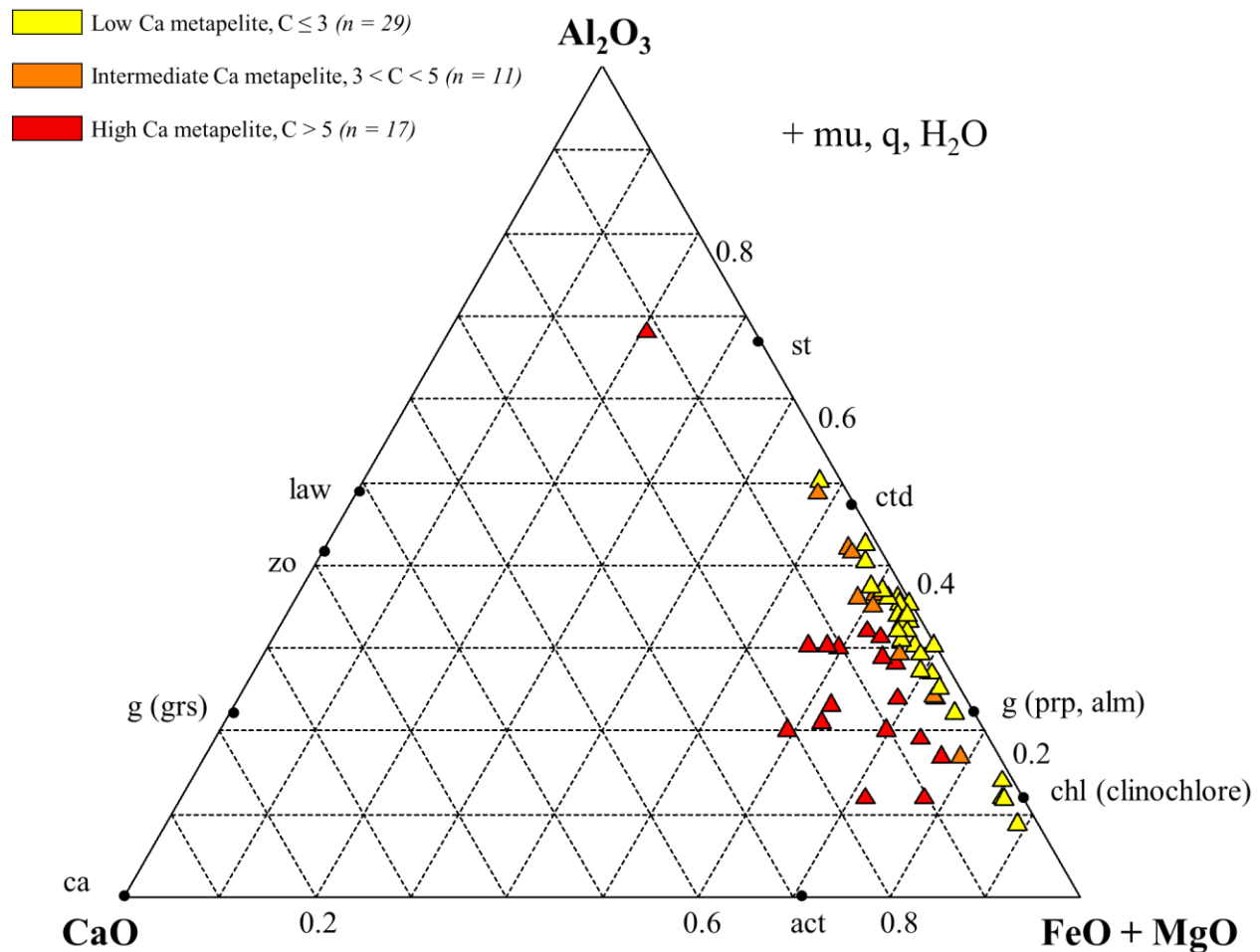


Figure 21. ACFM diagram showing all samples ($n=57$) from the continental domain. Data plotted using the subdivision low Ca metapelite, $C \leq 3$, intermediate Ca metapelite, $3 < C < 5$, and high Ca metapelite, $C > 5$.

Oceanic domain

Most samples are low-Ca metapelites ($n=29$), followed by high-Ca ($n=17$) and intermediate-Ca ($n=11$) metapelites (Figure 22). The intermediate Ca metapelites are mainly aluminous-rich ($A>0.25$), whereas the low and high Ca metapelites display high variability in their aluminous content ($0.01<A<0.8$).

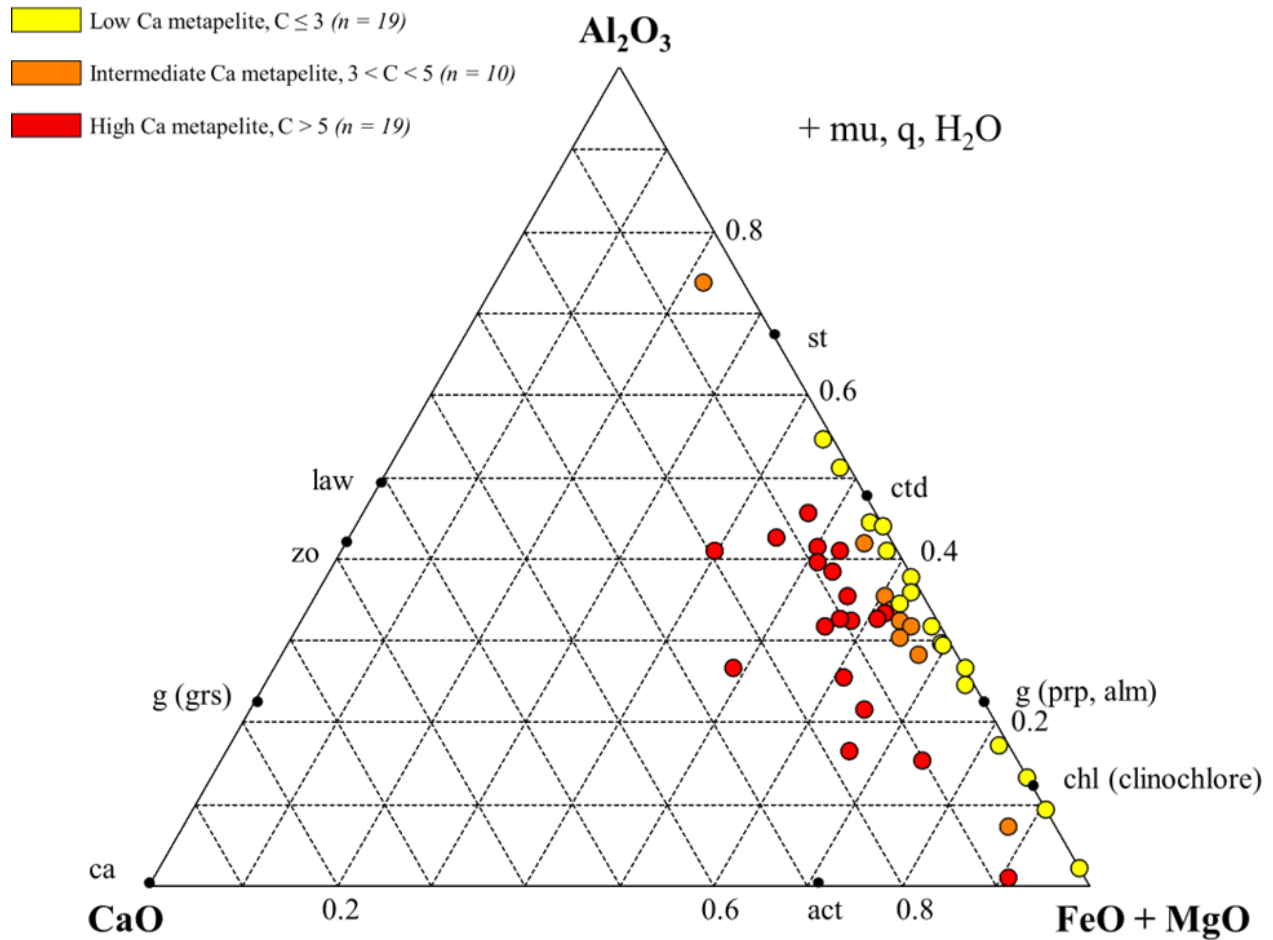


Figure 22. ACFM diagram showing all samples ($n=48$) from the Eastern Alps. Data plotted using the subdivision low Ca metapelite, $C \leq 3$, intermediate Ca metapelite, $3 < C < 5$, and high Ca metapelite, $C > 5$.

3.5 *Metapelites in oceanic domains vs. European plate vs. Adriatic plate*

The majority of samples (n=48) considered in this study are from oceanic domains (i.e., Piemonte Liguria ocean, Valais Basin and Tauern Window), followed by samples from the European plate (n=41); and the Adriatic plate (n=16) (Figure 23).

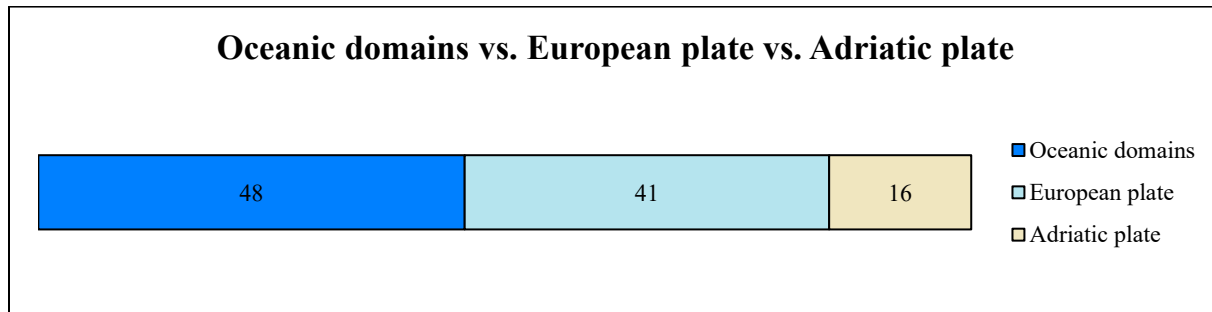


Figure 23. Chart showing the distribution of metapelites from the oceanic domains (Piemonte-Liguria Ocean, Valais Basin, Tauern Window), the European and Adriatic plates.

AFM

Overall, it is evident from Figure 24 that the data from the oceanic domains and the European plate are more dispersed than the ones from the Adriatic plate. The latter form a nice cluster in the domain of the aluminous-rich pelites.

All groups contain aluminous-rich metapelites ($A > 0.25$). Only the oceanic domains and the European plate show a few aluminous-poor metapelites (7 out of 48 and 6 out of 41, respectively; Figure 24). Samples from these two groups also display the biggest variation in their alumina content ($0.01 < A < 0.8$ and $0.1 \leq A < 0.8$, respectively). By contrast, the alumina content of metapelites from the Adriatic plate is comprised in a narrow range ($0.2 < A < 0.4$).

The M/FM ratios of samples belonging to the oceanic domains and European plates are variable, in the range 0.02–0.5 (Figure 24). By contrast, the M/FM ratios of samples from the Adriatic plate are in the range 0.15–0.38. Despite the similar M/FM ratio between the samples from the oceanic domain and the European plate, it is important to note that samples from the oceanic domain display higher F ($6 \leq F < 71$) and M ($5 \leq M < 63$) values than the samples from the continental domains.

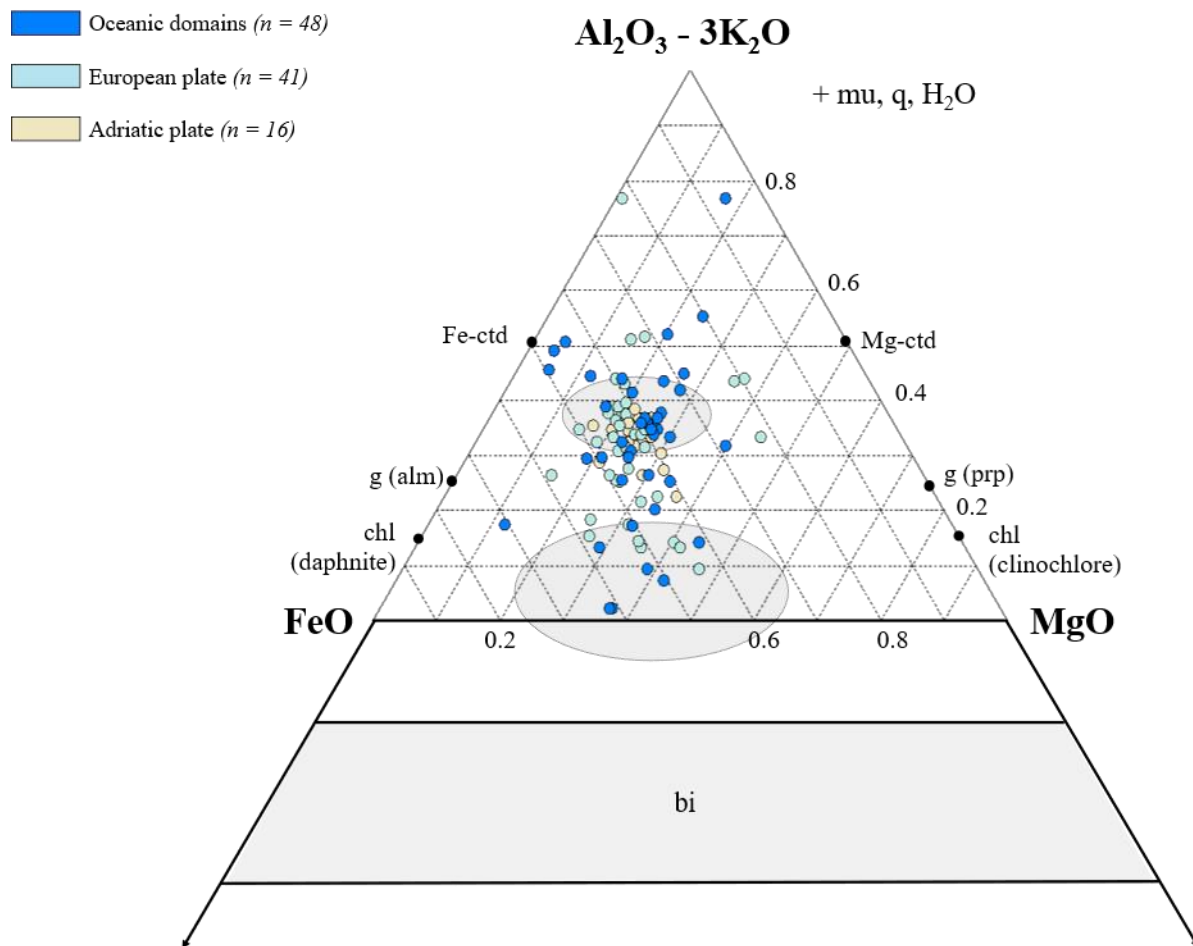


Figure 24. AFM diagram showing all samples ($n=105$) of metapelites sorted by oceanic domains (Piemonte-Liguria Ocean, Valais Basin, and Tauern Window Ocean), European plate and Adriatic plate.

ACFM

Oceanic domains

Samples are evenly divided between low Ca metapelites ($n=19$) and high Ca metapelites ($n=19$) (Figure 25). Intermediate Ca metapelites are the minority ($n=10$) and are mostly aluminous-rich ($A>0.25$) with only 1 out of 9 samples showing $A<0.25$. By contrast, both the low Ca metapelites ($0<A<0.6$) and high Ca metapelites ($0<A<0.5$) show a wider variability in their alumina content.

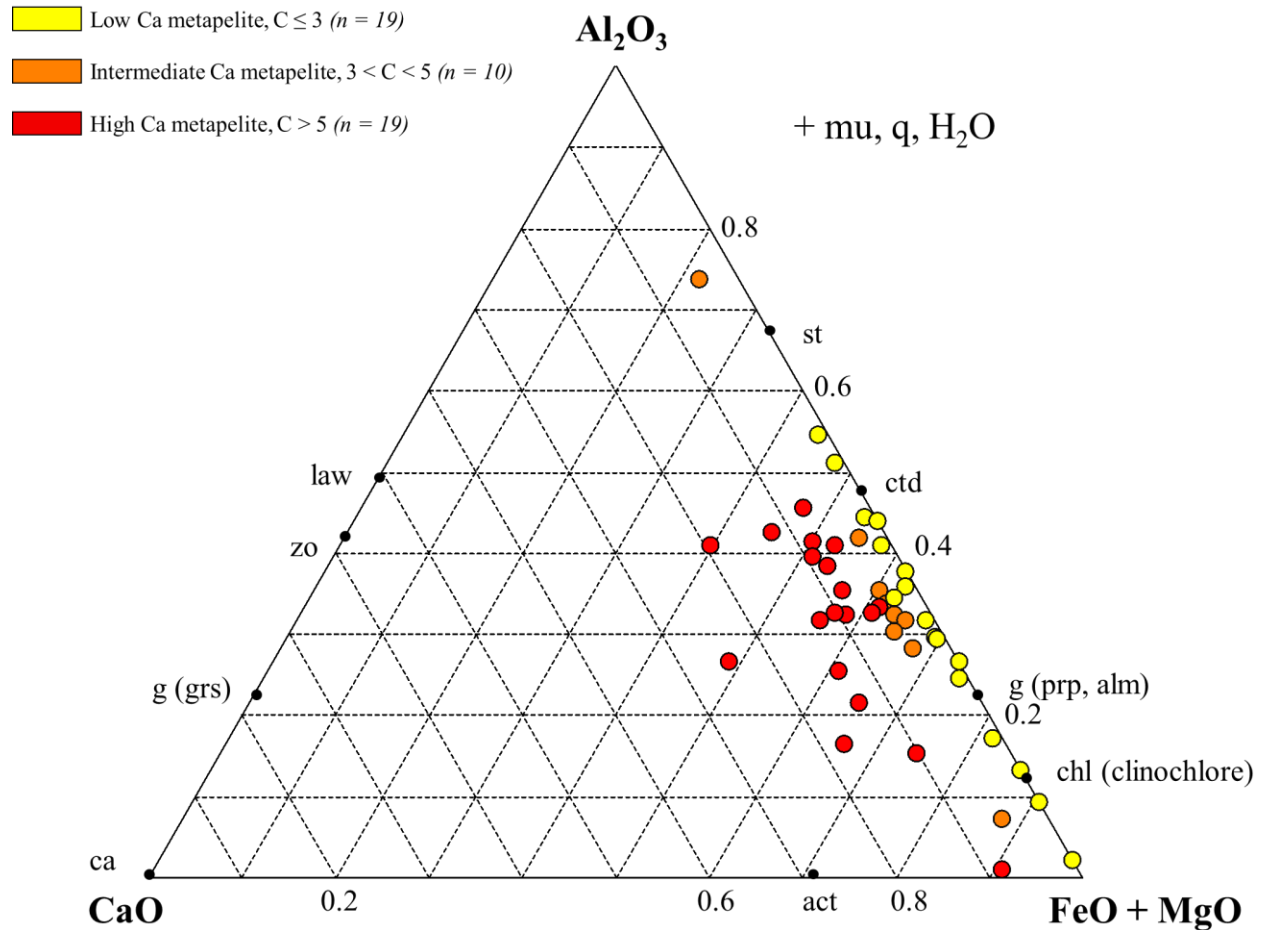


Figure 25. ACFM diagram showing all samples ($n=48$) from the oceanic domains (Piemonte-Liguria Ocean and Valais Basin + Tauern Window Ocean). Data plotted using the subdivision low Ca metapelite, $C \leq 3$, intermediate Ca metapelite, $3 < C < 5$, and high Ca metapelite, $C > 5$.

European plate

The majority of samples are low Ca metapelites ($n=22$), followed by high Ca ($n=10$) and intermediate Ca ($n=9$) metapelites (Figure 26). Low and intermediate Ca metapelites show a narrow Ca variability in comparison to the high Ca metapelites ($5 < C < 25$). In addition, low and intermediate Ca metapelites show a similar range of alumina content ($0 < A < 0.55$). By contrast, the high Ca metapelites show a wider variability in their alumina content ($0.1 < A < 0.7$).

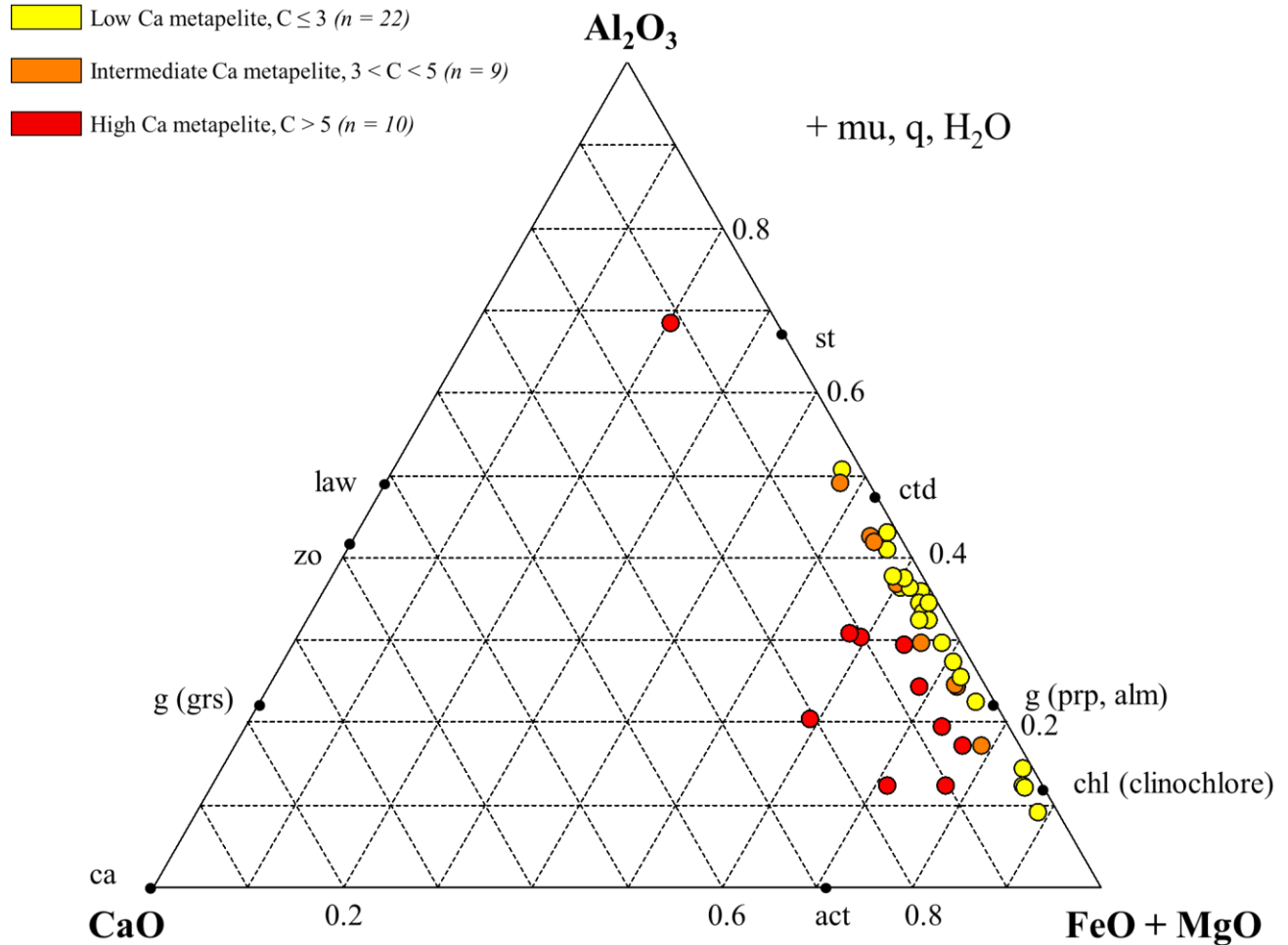


Figure 26. ACFM diagram showing all samples ($n=41$) from the European plate. Data plotted using the subdivision low Ca metapelite, $C \leq 3$, intermediate Ca metapelite, $3 < C < 5$, and high Ca metapelite, $C > 5$.

Adriatic plate

Samples are evenly distributed between low Ca metapelites ($n=7$) and high Ca metapelites ($n=7$, Figure 27). The high Ca metapelites also show a wide range of Ca concentrations ($5 < C < 20$). Both intermediate-Ca metapelites ($n=2$) and low Ca metapelites are aluminous-rich ($A > 0.25$). By contrast, high Ca metapelites show variability in aluminous concentrations ($0.15 < A < 0.45$).

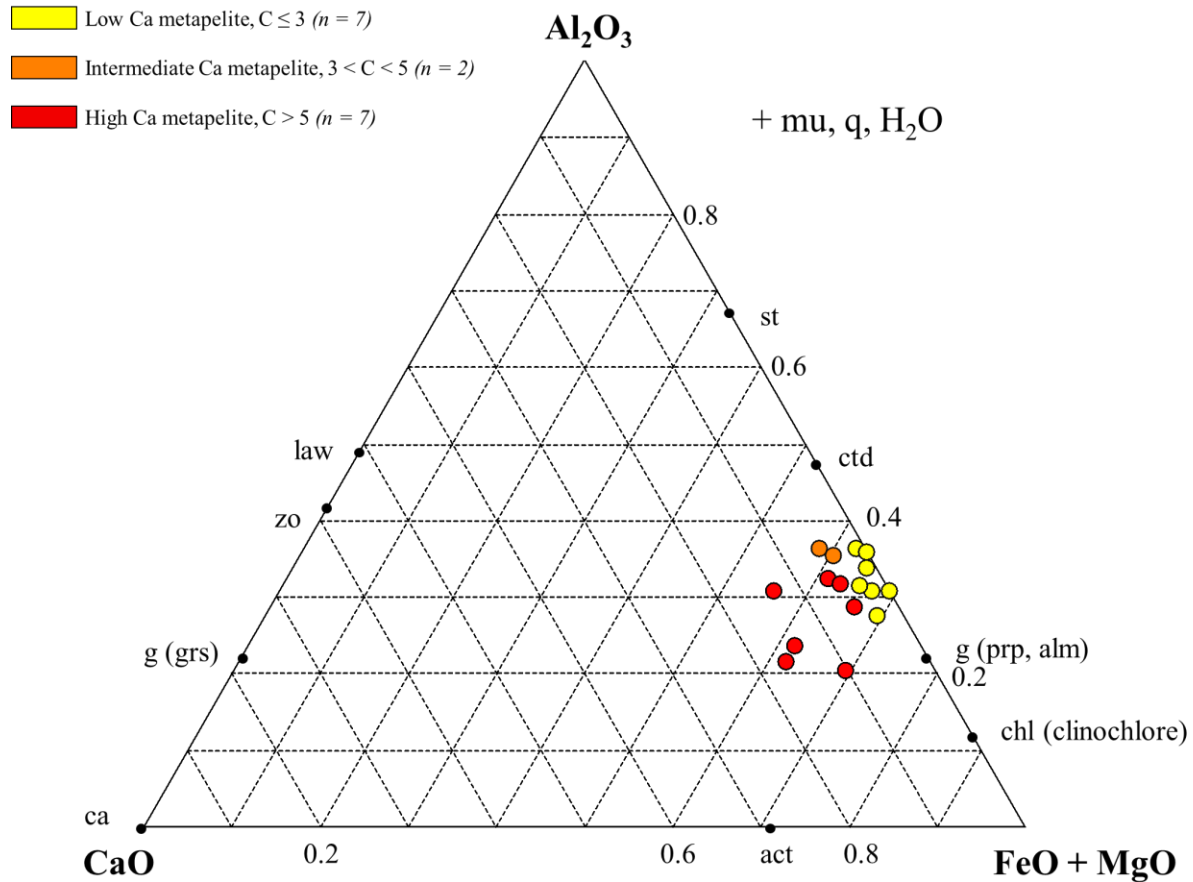


Figure 27. ACFM diagram showing all samples ($n=16$) from the European plate. Data plotted using the subdivision low Ca metapelite, $C \leq 3$, intermediate Ca metapelite, $3 < C < 5$, and high Ca metapelite, $C > 5$.

3.6 Metapelites in different geological units in the Alps

Most samples considered in this study are from the Upper Penninic nappes (n=41), followed by samples from the Middle Penninic nappes (n=20), the Southern Alps (n=16), the Sub-Penninic nappes (n=12), the Austroalpine nappes (n=10), the Lower Penninic nappes (n=5), and Sesia-Margna nappes (n=1) (Figure 28).

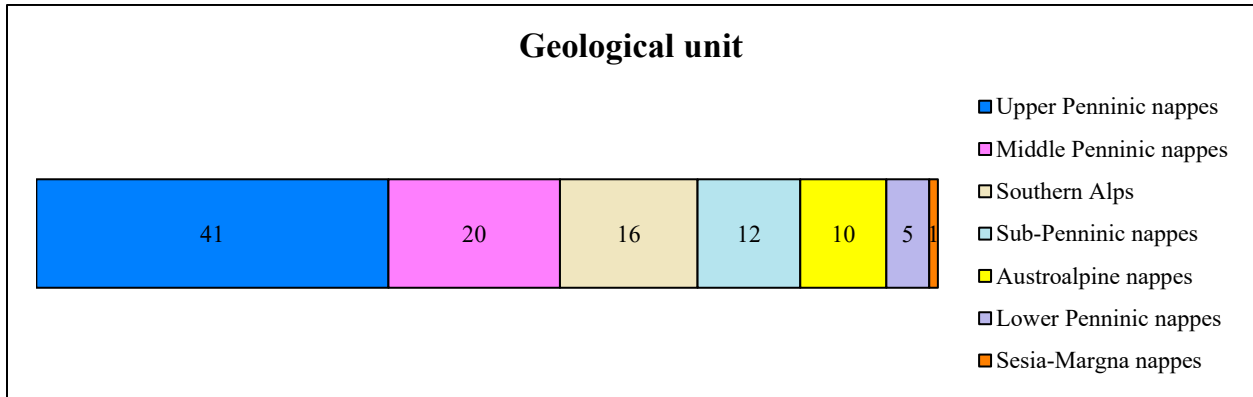


Figure 28. Chart showing the distribution of metapelites according to their geological Alpine units.

AFM

All units contain aluminous-rich pelites, but only the Upper and the Middle Penninic nappes also display a few aluminous-poor pelites (6 out of 41 and 7 out of 20 samples, respectively; Figure 29). In details, most samples from the Austroalpine nappes, the Southern Alps, the Sub-Penninic nappes, and the Lower Penninic nappes are aluminous-rich ($A > 0.25$). The sample from the Sesia-Margna nappes ($n=1$) is also aluminous-rich. By contrast, samples from the Upper Penninic nappes and the Middle Penninic nappes show variability in their aluminous content ($0.01 < A < 0.75$ and $0.1 < A < 0.5$, respectively).

Metapelites from all geological units display variable M/FM ratio. The largest variability is shown by samples belonging to the Upper Penninic nappes (0.05–0.45), Sub-Penninic nappes (0.1–0.45), and Middle Penninic nappes (0.15–0.5). Samples from the Austroalpine nappes and Southern Alps have a M/FM ratio in the range 0.15–0.32 and 0.15–0.35, respectively. Sample from the Sesia-Margna nappes displays the lowest M/FM ratio (0.02), whereas the M/FM ratios of samples from the Lower Penninic nappes are comprised between 0.1 and 0.4.

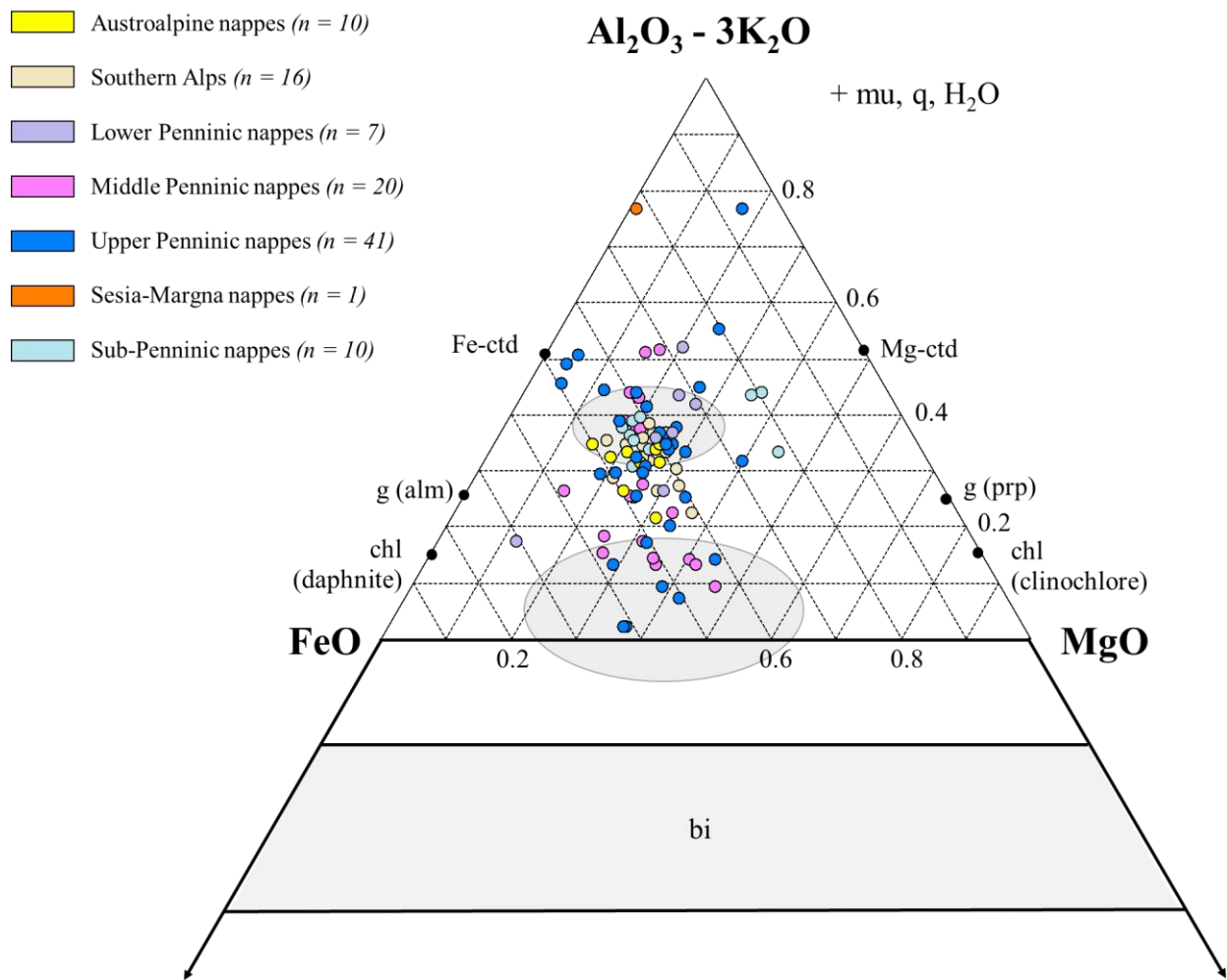


Figure 29 AFM diagram showing all samples ($n=105$) plotted as a function of the geological unit to which they belong.

ACFM

The sample from the Sesia-Margna (n=1) is a high Ca metapelite ($C > 5$) (Figure 30), whereas samples from all the other units display large variability in their Ca content and fall in the group of low ($C \leq 3$), intermediate ($3 < C < 5$), and high Ca metapelites ($C > 5$).

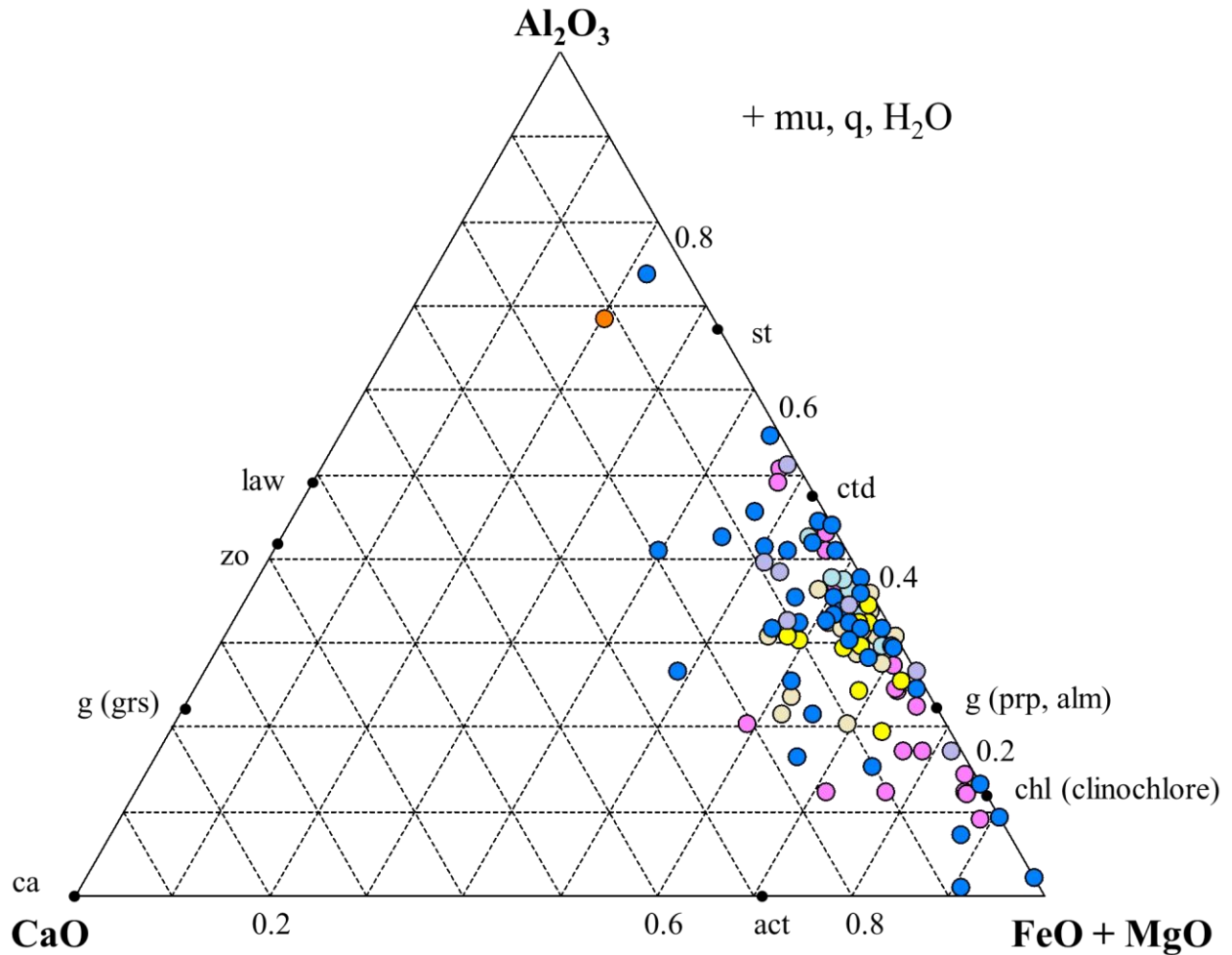


Figure 30. ACFM diagram showing all samples (n = 105) plotted as a function of the geological unit to which they belong.

3.7 Metapelites in the Alps and their metamorphic conditions

In the following diagrams, metapelites are plotted as a function of their metamorphism. For convenience, we adopt the metamorphic facies subdivision, following the correspondence between mineral facies and the mineral assemblages developed in metapelites as proposed by Manzotti and Ballèvre 2024 (see Table 2 in the Appendix).

The majority of samples (n=33) considered in this study record amphibolite facies metamorphism, followed by blueschist (n=29), eclogite (n=24), coe-eclogite (n=7), greenschist (n=6), and granulite facies (n=6) (Figure 31).

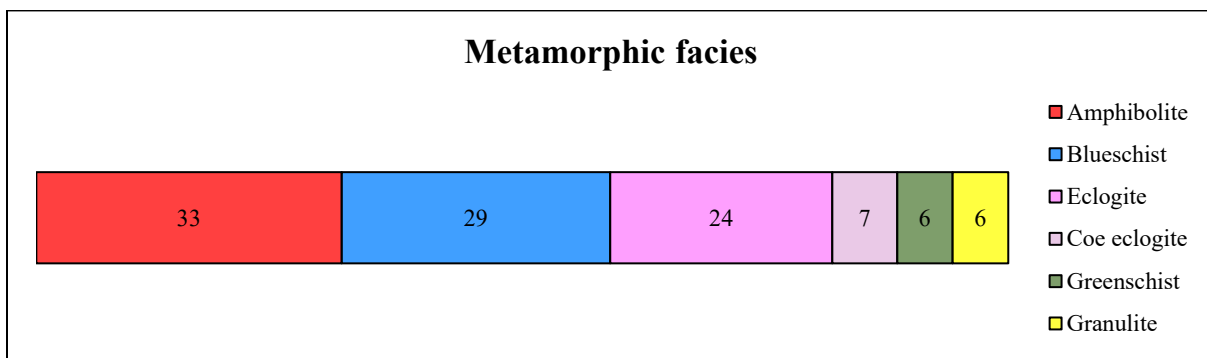


Figure 31. Chart showing the distribution of metapelites sorted by metamorphic facies.

AFM

Considering the metamorphic criterion, it appears that aluminous-rich metapelites are present in all metamorphic facies groups, but a large cluster of aluminous-rich metapelites falls in the amphibolite facies group (Figure 32). Aluminous poor metapelites belong to the groups of coe-eclogite (n= 3), eclogite (n=6), and blueschist facies (n=5).

In detail, the aluminous-rich metapelites are dominated by samples belonging to the amphibolite, blueschist, greenschist and granulite facies groups ($A > 25$). Samples belonging to the blueschist ($0 < A < 0.8$) and eclogite ($0 < A < 0.7$) groups displays the largest variability in their alumina content. By contrast, the smallest variability in the alumina content is shown by samples belonging to the granulite facies group ($0.2 < A < 0.4$).

Most of the groups displays a large variability in the M/FM ratio (eclogite: 0.02–0.5; coe-eclogite: 0.15–0.45; amphibolite: 0.15–0.45; blueschist facies: 0.05–0.42). By contrast, the greenschist and the granulite groups show the smallest variability in their M/FM ratio (i.e. 0.2–0.3).

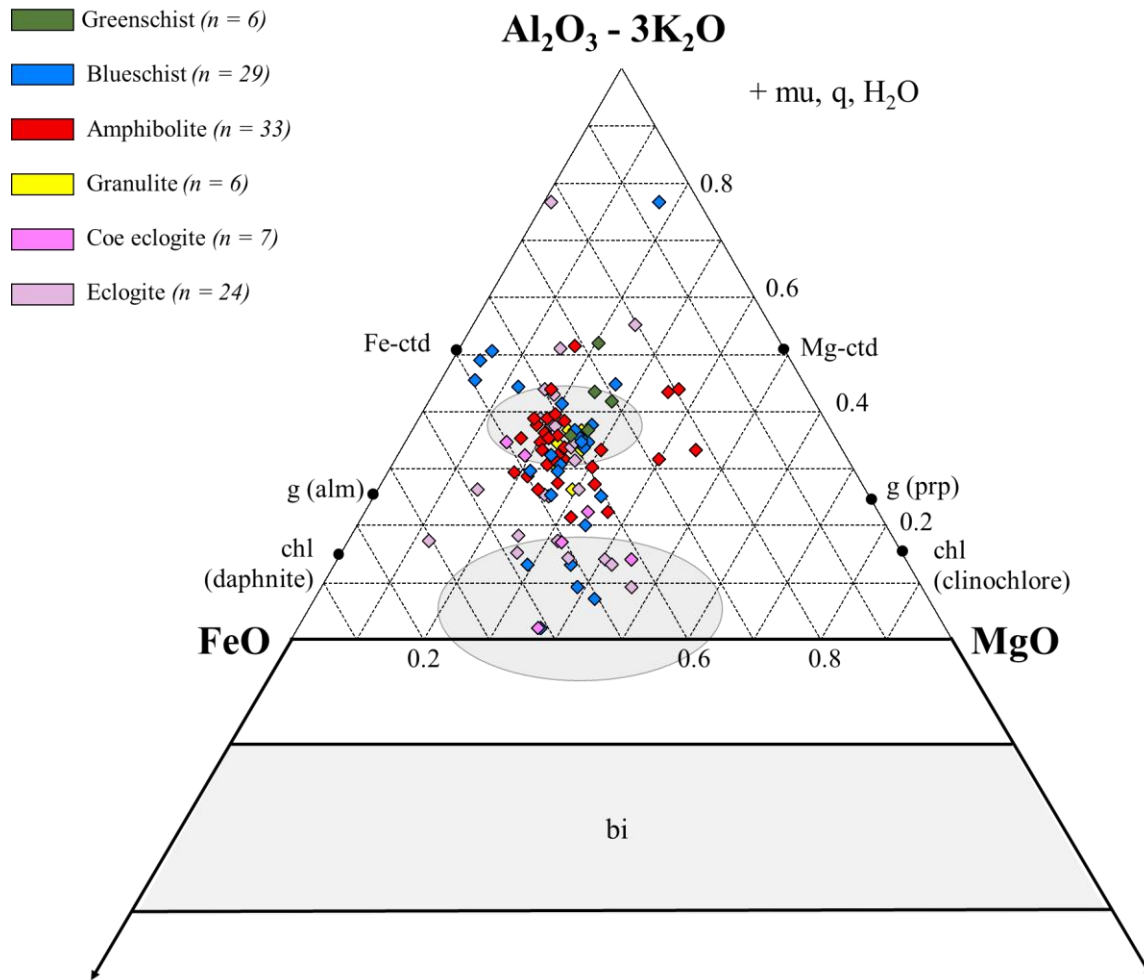


Figure 32. AFM diagram showing all samples (n=105) plotted as a function of metamorphic facies.

ACFM

All the metamorphic facies groups contain low Ca ($C \leq 3$), intermediate Ca ($3 < C < 5$) and high Ca ($C > 5$) metapelites (Figure 33). If we consider for example the greenschist facies group ($n=6$), it comprises 2 low Ca, 2 intermediate and 2 high Ca metapelites). The groups of amphibolite ($0 < C < 16$), blueschist ($0 < C \leq 25$), eclogite ($0 < C < 22$), and granulite ($0 < C < 20$) display very variable Ca content. Low-Ca and intermediate-Ca metapelites are dominant in the amphibolite, granulite, blueschist and eclogite facies groups.

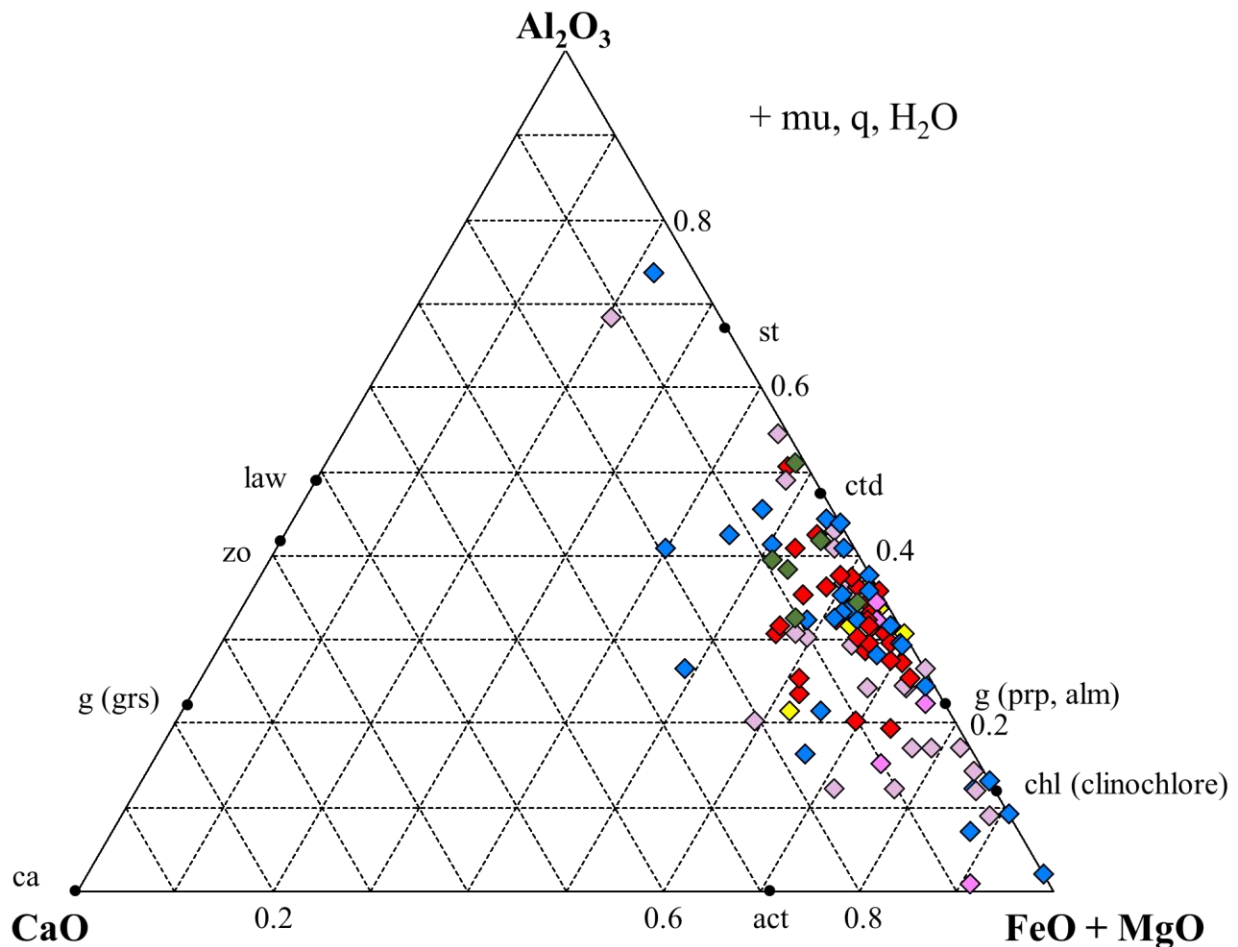


Figure 33. ACFM diagram showing all samples ($n=105$) plotted as a function of metamorphic facies.

4. Discussion and conclusions

This study investigates the variability of bulk rock composition of metapelites in the Alpine realm, on the basis of a literature compilation of 105 bulk composition data. Data were plotted in AFM and ACFM diagrams according to the following criteria:

- Geographic position
- Oceanic vs. continental affinity
- Geological unit
- Metamorphic facies

In the following, the main results derived from this work are briefly discussed and used to draw a few conclusions. It is important to highlight that the built dataset is quite limited ($n = 105$) with respect to the large amount of metapelites present in the Alpine belt. In addition, a variable number of data is available for the different groups. For example, data from the Western Alps are more numerous than the ones from the Central and Eastern Alps. Furthermore, the bulk rock compositions were estimated using three different methods, potentially introducing some intrinsic discrepancies related to the accuracy and precision of the used method. Therefore, we are aware that these factors may partially bias some of the conclusions.

4.1 *Bulk rock chemistry of Alpine metapelites and comparison with other belts*

The majority of samples (87 out of 105) are aluminous-rich Ca-poor metapelites ($A > 0.25$, $C < 3$). In detail, Alpine metapelites display variable M/FM ratios (in the range 0.02–0.5) and Ca content, with a majority of low-Ca metapelites ($n=48$) followed by high-Ca and intermediate Ca metapelites ($n=36$ and $n=21$, respectively). The presence of intermediate- to high-CaO metapelites suggests input from carbonate-bearing sedimentary rocks at the time of sedimentation.

These observations are in line with the study of Forshaw and Pattison (2023). These authors compared the bulk rock composition of metapelites in several orogenic belts (Figure 34a), but did not explore in detail the Ca content of metapelites, as this thesis tentatively attempts. The database built from Forshaw and Pattison (2023) consists only of metapelites that experience medium pressure to low pressure metamorphism. The dataset built in this thesis also includes metapelites affected by high pressure to ultra-high pressure metamorphism. The latter is widespread in the Alpine belt, especially in the Western Alps (Manzotti and Ballèvre 2024). Comparison of the bulk rock compositions of Alpine metapelites equilibrated at different metamorphic grade well shows that aluminous-rich metapelites as well as low, intermediate, and high Ca metapelites are present in all metamorphic facies' groups in the Alps. This observation proves that metamorphism (changes in P and T conditions) can affect rocks of any different composition.

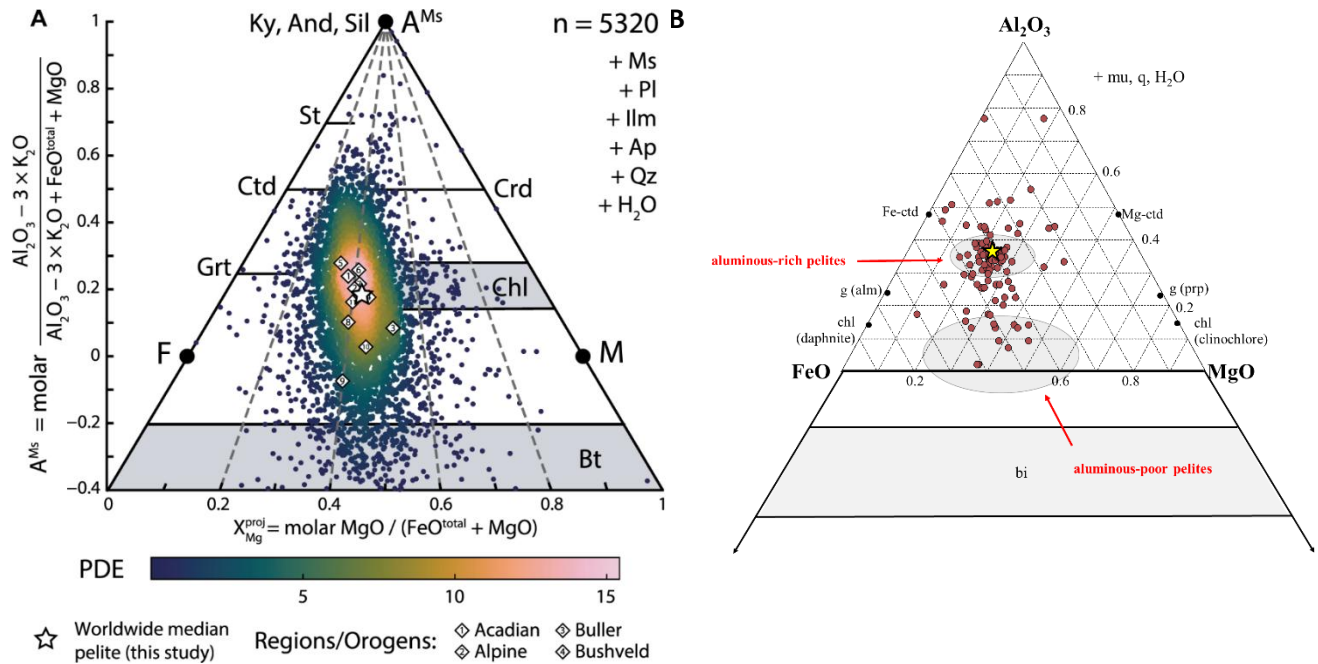


Figure 34. (a) AFM diagram showing metapelites from different orogenic belts ($n=5320$, Forshaw and Pattison 2023). The number 2 is the median composition of metapelites from the Alpine belt. (b) AFM diagram showing Alpine metapelites ($n=105$) considered in this study. The yellow star is the median composition of metapelites from the Alpine belt, calculated with the dataset built in this study (which also includes metapelites equilibrated at high pressure to ultra-high pressure metamorphism).

Forshaw and Pattison (2023) calculated (i) the composition for a median worldwide pelite (white star in Figure 34a) and (ii) the median composition for a metapelite from the Alpine belt, which corresponds to an aluminous-rich metapelite (indicated with number 2 in Figures 34a).

A median composition for a metapelite from the Alpine belt is calculated using the dataset built in this thesis (yellow star in Figure 34b) and is as follows:

$\text{SiO}_2 = 57.61$, $\text{TiO}_2 = 0.88$, $\text{Al}_2\text{O}_3 = 20.50$, $\text{FeO}_{\text{total}} = 8.20$, $\text{MnO} = 0.12$, $\text{MgO} = 2.39$, $\text{CaO} = 0.58$, $\text{Na}_2\text{O} = 1.03$, and $\text{K}_2\text{O} = 3.53$.

The median $X_{\text{Mg}} = \text{MgO}/(\text{MgO} + \text{FeO}_{\text{total}})$ in moles is 0.34.

This median composition is quite similar to the composition for a median worldwide pelite calculated by Forshaw and Pattison (2023, white star in Figure 34a). and to the one calculated by the same authors for the Alpine belt.

4.2 Bulk rock chemistry of metapelites across the Alpine belt

In the different sectors of the Alps (Western, Central, and Eastern), intermediate Ca metapelites are not very abundant. The Central and Eastern Alps mainly comprise aluminous-rich metapelites, whereas in the Western Alps, metapelites display a large variability in their alumina content. These differences may be linked to the large number of data available from the Western Alps compared to the Central and Eastern Alps. In this case, these differences do not reflect the real distribution across the belt. Alternatively, these differences may be related to the extraction of data from several geological units from the Western Alps with respect to the Central and Eastern Alps (see Table 1 and Figure 7). In other words, the largest variability in alumina content may reflect the different sources of the sediments at the time of deposition.

4.3 Bulk rock chemistry of metapelites: oceanic domain vs. Adriatic plate vs. European plate

Aluminous-rich metapelites ($A > 25$) are abundant in the oceanic domains (Piemonte-Liguria Ocean and Valais Basin) as well as in the Adriatic and European plates. In the Alps, aluminous-poor metapelites are scarce and found only in the oceanic domains and in the European plate. Metapelites from the Adriatic plate ($n=16$) display minor variation in their alumina content ($0.2 < A < 0.4$) and M/FM ratio ($0.15-0.38$) and form a cluster in correspondence of the composition of alumina-rich metapelites. This may indicate (i) a more restricted source of sediments or (ii) sources of sediments that are homogenous.

With respect to the Ca content, Ca-rich metapelites are less abundant in the European plate than in the oceanic domains and Adriatic plate. However, given the few data available from the Adriatic plate ($n=16$) compared to the oceanic domains and European plate ($n=48$ and $n=41$, respectively), we cannot exclude that Ca-poor metapelite in the Adriatic plate are underrepresented in our dataset.

The largest variation in chemistry (e.g. A, F, M, and C) is shown by samples from the oceanic domains (both Upper and Lower Penninic nappes). Interestingly, the M/FM ratios of samples belonging to both the oceanic domains and European plates are variable, in the range $0.02-0.5$. However, despite the similar M/FM ratio, metapelites from the oceanic domains display higher F ($6 \leq F < 71$) and M ($5 \leq M < 63$) values than the samples from the European plate. Metapelites from these domains display characteristic geochemical markers of material from oceanic provenance, which include high FeO and MgO contents and lower Al_2O_3 when compared to their continental counterparts. This may suggest that the sediments accumulated were influenced by mafic and/or ultramafic detrital input as opposed to clay-rich material deposited in continental basins. The variability of the geochemistry of these samples supports the idea that these units originated from specific depositional environments which range from deep-sea pelagic sediments to more iron-rich material which is typically associated with mid-ocean ridges.

4.4 Bulk rock chemistry of metapelites in different geological units

A comparison of the bulk rock chemistry of metapelite from different geological units in the Alps is complex, because there is an enormous disparity in the number of data available in each unit. The unit with the large number of data is the Upper Penninic nappes (n=41, Piemonte-Liguria Ocean), whereas the one with the smallest number of data is the Sesia-Margna nappes (n=1, Adriatic plate). Therefore, only a few considerations are made.

In the Adriatic plate (Austroalpine nappes, Southern Alps, and Sesia-Margna nappes), metapelites are aluminous-rich. While the M/FM ratios of samples from the Austroalpine nappes and Southern Alps are comparable and comprised in the range 0.15–32, the M/FM ratio of the unique sample available from the Sesia-Margna nappes is extremely low (0.02). Given that there is only one data from the Sesia-Margna nappes, this result is not statistically significant. However, further investigations are needed to clarify a potential difference.

The larger compositional variability (alumina and Ca content, M/FM ratio) is observed for the samples belonging to the Upper Penninic nappes (i.e. the best represented, n=41) and the Middle Penninic nappes (n=20). The latter is interpreted as a microcontinent derived from the European palaeomargin and experienced eclogite-facies metamorphism during the Alpine history. The observed variability in these domains may be explained by heterogenous sources of sediments.

5. Future work

While this study contributes to a general understanding into the makeup of bulk rock composition of metapelites within the Alpine realm, it is still lacking due to inevitable biases. Future work can include a study of a better representation of samples that encompasses the same number of samples from more regions in the Alpine realm. This could give us a more representative result without the flaw of bias for a specific location, which would lead to a more thorough and extensive understanding of bulk rock composition of metapelites in the Alps. In addition, the built dataset comprises a few outliers (e.g., a few metapelites extremely rich in alumina) that need a better characterization.

6. Acknowledgments

I would like to express my deepest gratitude to my professor and supervisor for her excellent guidance, patience and feedback.

Lastly, I'd like to mention my family, significant other and friends for keeping me motivated, high-spirited and for supporting me through this project.

7. References

1. Agard P (1999). Evolution métamorphique et structurale des métapelites océanique dans l'orogène alpin: l'exemple des schistes lustrés des Alpes occidentales (Alpes Cottiennes). *Pétrographie*. Université Pierre et Marie Curie – Paris VI.
2. Ali A, Zhang N, Santos RM (2023). Mineral characterization using scanning electron microscopy (SEM): a review of the fundamentals, advancements, and research directions. *Applied Sciences*, 13, 12600.
3. Angiboust S, Langdon R, Agard P, Waters D, Chopin C (2012). Eclogitization of the Monviso ophiolite (W. Alps) and implications on subduction dynamics. *Journal of Metamorphic Geology*, 30, 37-61, <https://doi.org/10.1111/j.1525-1314.2011.00951.x>.
4. Bebout GE, Agard P, Kobayashi K, Moriguti T, Nakamura E (2013) Devolatilization history and trace element mobility in deeply subducted sedimentary rocks: Evidence from Western Alps HP/UHP suites. *Chemical Geology*, 342, 1-20, <https://doi.org/10.1016/j.chemgeo.2013.01.009>.
5. Braga R, Massonne HJ (2012). H₂O content of deep-seated orogenic continental crust: the Ulten Zone, Italian Alps. *International Geology Review*, 53, 633-641, <https://doi.org/10.1080/00206814.2010.548155>.
6. Brovarone AV, Picatto M, Beyssac O, Lagabrielle Y, Castelli D (2014). The blueschist-eclogite transition in the Alpine chain: P-T paths and the role of slow-spreading extensional structures in the evolution of HP-LT mountain belts. *Tectonophysics*, 615-616, 96-121, <https://doi.org/10.1016/j.tecto.2014.01.001>.
7. CRAIC Technologies. GeoImage Point Counting. Available from: <https://www.microspectra.com/products/geoimage?highlight=WyJnZW9pbWFnZSJd#point-counting>.
8. Epstein GS, Bebout GE, Angiboust S, Agard P (2019). Scales of fluid-rock interaction and carbon mobility in the deeply underplated and HP-Metamorphosed Schistes Lustrés, Western Alps. *Lithos*, 354-355, 105229, <https://doi.org/10.1016/j.lithos.2019.105229>.
9. Forshaw JB, Pattison DR (2023). Major-element geochemistry of pelites. *Geology*, 51, 39-43.
10. Gaidies F, Abart T, De Capitani C, Schuster R, Connolly JA, Reusser E (2006). Characterization of polymetamorphism in the Austroalpine basement east of the Tauern Window using garnet isopleth thermobarometry. *Journal of Metamorphic Geology*, 24, 451–475, <https://doi.org/10.1111/j.1525-1314.2006.00648.x>.
11. Garfalo PS (2012). The composition of Alpine marine sediments (Bündnerschiefer Formation, W Alps) and the mobility of their chemical components during orogenic metamorphism. *Lithos*, 128-132, 55-72, <https://doi.org/10.1016/j.lithos.2011.10.009>.
12. Ghignone S, Scaramuzzo E, Bruno M, Livio FA (2023). A new UHP unit in the Western Alps: First occurrence of coesite from the Monviso Massif (Italy). *American Mineralogist*, 108, 1368-1375, <https://doi.org/10.2138/am-2022-8621>.

13. Gierre R, Rumble D, Günther D, Connolly J, Caddick MJ (2011). Correlation of Growth and Breakdown of Major and Accessory Minerals in Metapelites from Campolungo, Central Alps. *Journal of Petrology*, 53, 2293-2334, <https://doi.org/10.1093/petrology/egr043>.
14. Gill P (1997). *Modern Analytical Geochemistry: an introduction to quantitative chemical analysis techniques for Earth, environmental and materials scientists*. Routledge, ISBN: 9780582099449.
15. Groppo C, Ferrando S, Gilio M, Botta S, Nosenzo F, Balestro G, Festa A, Rolfo F (2019). What's in the sandwich? New P-T constraints for the (U)HP nappe stack of southern Dora-Maira Massif (Western Alps). *European Journal of Mineralogy*, 31, 665-68, <https://doi.org/10.1127/ejm/2019/0031-2860>.
16. Groppo C, Ferrando S, Tursi F, Rolfo F (2025). A new UHP-HP Tectono-Metamorphic Architecture for the Southern Dora-Maira Massif Nappe Stack (Western Alps) Based on Petrological and Microstructural Evidence. *Journal of Metamorphic Geology*, 43, 359-383, <https://doi.org/10.1111/jmg.12812>.
17. Henry C, Burkhard M, Goffé B (1996). Evolution of synmetamorphic veins and their wallrocks through a Western Alps transect: no evidence for large-scale fluid flow. Stable Isotope, major- and trace-element systematics. *Chemical Geology*, 127, 81-109, [https://doi.org/10.1016/0009-2541\(95\)00106-9](https://doi.org/10.1016/0009-2541(95)00106-9).
18. Hoschek G, Konzett J, Tessadri R (2010). Phase equilibria in quartzitic garnet-kyanite-chloritoid micaschist from the Eclogite Zone, Tauern Window, Eastern Alps. *European Journal of Mineralogy*, 22, 721-732, <https://doi.org/10.1127/0935-1221/2010/0022-2049>.
19. Hurai V, Janák M, Thomas R (2010). Fluid-assisted retrogression of garnet and P-T history of metapelites from HP/UHP metamorphic terrane (Pohorje Mountains, Eastern Alps). *Contributions to Mineralogy and Petrology*, 160, 203-218, <https://doi.org/10.1007/s00410-009-0473-7>.
20. Janots E, Engi M, Berger A, Allaz J, Schwarz JO, Spandler C (2008). Prograde metamorphic sequence of REE minerals in pelitic rocks of the Central Alps: implications for allanite–monazite–xenotime phase relations from 250 to 610 °C. *Journal of Metamorphic Geology*, 26, 509-526, <https://doi.org/10.1111/j.1525-1314.2008.00774.x>.
21. Keller L. M, Abart R, Stünitz H, De Capitani C (2004). Deformation, mass transfer and mineral reactions in an eclogite facies shear zone in a polymetamorphic metapelite (Monte Rose nappe, Western Alps). *Journal of Metamorphic Geology*, 22, 97-118, <https://doi.org/10.1111/j.1525-1314.2004.00500.x>.
22. Klein C, Philpotts AR (2017). *Earth Materials: Introduction to Mineralogy and Petrology*. Cambridge University Press, ISBN: 978-0521145213.
23. Kuisma-Kursula P (2000). Accuracy, precision and detection limits of SEM–WDS, SEM–EDS and PIXE in the multi-elemental analysis of medieval glass. *X-Ray Spectrometry: An International Journal*, 29, 111-8.

24. Le Bayon B, Pitra P, Ballèvre M, Bohn M (2006). Reconstructing P-T paths during continental collision using multi-stage garnet (Gran Paradiso nappe, Western Alps). *Journal of Metamorphic Geology*, 24, 477–496.
25. Li B, Massonne HJ, Koller F, Zhang J (2021). Metapelite from the high- to ultrahigh-pressure terrane of the Eastern Alps (Pohorje Mountains, Slovenia) – New pressure, temperature and time constraints on a polymetamorphic rock. *Journal of Metamorphic Geology*, 39, 695–726, <https://doi.org/10.1111/jmg.12581>.
26. Manzotti P, Ballèvre M (2024). Continental subduction in the Alps: from field data to kinematic models. Chapter 5, v.2, 255–313, in “Geodynamics of the Alps”, Eds: Rosenberg C, Bellahsen N, Sciences – Dynamics of the continental lithosphere, Wiley, ISBN: 9781789451160, DOI: 10.1002/9781394299539.ch5.
27. Manzotti P, Ballèvre M, Pitra P, Schiavi F (2021). Missing lawsonite and aragonite found: P-T and fluid composition in meta-marls from the Combin Zone (Western Alps). *Contributions to Mineralogy and Petrology*, 176, 60, <https://doi.org/10.1007/s00410-021-01818-0>.
28. Manzotti P, Bosse V, Pitra P, Robyr M, Schiavi F, Ballèvre M (2018). Exhumation rates in the Gran Paradiso Massif (Western Alps) constrained by in situ U–Th–Pb dating of accessory phases (monazite, allanite and xenotime). *Contributions to Mineralogy and Petrology*, 173, 1–28. <https://doi.org/10.1007/s00410-018-1452-7>.
29. Manzotti P, Schiavi F, Nosenzo F, Pitra P, Ballèvre M (2022). A journey towards the forbidden zone: a new, cold, UHP unit in the Dora-Maira Massif (Western Alps). *Contributions to Mineralogy and Petrology*, 177, 59, <https://doi.org/10.1007/s00410-022-01923-8>.
30. Miron GD, Wagner T, Wälle M, Heinrich CA (2013). Major and trace-element composition and pressure-temperature evolution of rock-buffered fluids in low-grade accretionary-wedge metasediments, Central Alps. *Contributions to Mineralogy and Petrology*, 165, 981–1008, <https://doi.org/10.1007/s00410-012-0844-3>.
31. Nelson SA (2011). *Triangular Plots in Metamorphic Petrology*. Sitio web de la Universidad Tulane, Nueva Orleans.
32. Nosenzo F, Manzotti P, Robyr M (2023). H₂O budget and metamorphic re-equilibration in polycyclic rocks as recorded by garnet textures and chemistry. *Lithos*, 452–453, 107230, <https://doi.org/10.1016/j.lithos.2023.107230>.
33. Petrelli M, Poli G, Perugini D, Peccerillo A (2005). PetroGraph: A new software to visualize, model, and present geochemical data in igneous petrology. *Geochemistry, Geophysics, Geosystems*, 6, <https://doi.org/10.1029/2005GC000932>.
34. Pfiffner OA. *The structure of the Alps: an introduction* (1993). Pre-Mesozoic Geology in the Alps 1993, 3–5, Berlin, Heidelberg: Springer Berlin Heidelberg.
35. Ramsey MH, Potts PJ, Webb PC, Watkins P, Watson JS, Coles BJ (1995). An objective assessment of analytical method precision: comparison of ICP-AES and XRF for the analysis of silicate rocks. *Chemical Geology* 124, 1–9.

36. Redler C, Irouschek A, Jeffries T, Gieré R (2016). Origin and formation of Tourmaline-rich cordierite-bearing metapelitic rocks from Alpe Sponda, Central Alps (Switzerland). *Journal of Petrology*, 57, 277-308, <https://doi.org/10.1093/petrology/egw006>.
37. Redler C, Johnson TE, White RW, Kunz BE (2012). Phase equilibrium constraints on a deep crustal metamorphic field gradient: metapelitic rocks from the Ivrea Zone (NW Italy). *Journal of Metamorphic Geology*, 30, 235-254, <https://doi.org/10.1111/j.1525-1314.2011.00965.x>.
38. Regis D, Rubatto D, Darling J, Cenko-Tok B, Zucali, M, Engi M (2014). Multiple Metamorphic Stages within an Eclogite-facies Terrane (Sesia Zone, Western Alps) Revealed by Th–U–Pb Petrochronology. *Journal of Petrology*, 55, 1429-1456, <https://doi.org/10.1093/petrology/egu029>.
39. Ross PS, Giroux B, Latutrie B (2021). Precision and accuracy of modal analysis methods for clastic deposits and rocks: A statistical and numerical modeling approach. *Geosphere*, 17, 987-1006.
40. Smye AJ, Greenwood LV, Holland TJ (2010). Garnet-chloritoid-kyanite assemblages: eclogite facies indicators of subduction constraints in orogenic belts. *Journal of Metamorphic Geology*, 28, 753-768, <https://doi.org/10.1111/j.1525-1314.2010.00889.x>.
41. Spear FS (1993). *Metamorphic phase equilibria and pressure–temperature–time paths*. Mineralogical Society of America Monograph, 352.
42. Stüwe K, Powell R (1995). PT Paths from modal proportions: application to the Koralm Complex, Eastern Alps. *Contributions to Mineralogy and Petrology*, 119, 83-93.
43. Tajčmanová L, Manzotti P, Alvaro M (2021). Under pressure: high-pressure metamorphism in the Alps. *Elements: An International Magazine of Mineralogy, Geochemistry, and Petrology*, 17, 17-22.
44. Winter, JD (2014). *Principles of Igneous and Metamorphic Petrology*. Harlow, UK, Pearson education.
45. Wyatt DC, Smye AJ, Garber JM, Hacker BR (2022). Assembly and Tectonic Evolution of Continental Lower Crust: Monazite Petrochronology of the Ivrea-Verbano Zone (Val Strona di Omegna). *Tectonics*, 41, e2021TC006841, <https://doi.org/10.1029/2021TC006841>.
46. Zou L, Guo JH, Huang GY, Jiao SJ, Tian ZH, Liu PH (2022). The effect of bulk rock composition in phase equilibria modelling: a case study of mafic granulites from the North China Craton. *Contributions to Mineralogy and Petrology*, 177, 22.

8. Appendix

Table 2: Metapelites in the Alps and their metamorphic conditions

Metamorphic facies	Metabasites	Metapelites
greenschist	ab-chl-act-ep	q-mu-chl q-mu-chl-bi
law blueschist	gl-law-ttn	q-mu-ctd-car-chl
ep blueschist	g-gln-ep-ru	q-mu-g-ctd-chl
law eclogite	law-cpx-g-ru	q-mu-g-ctd
ep eclogite am eclogite	g-cpx-ru-q-am-ep	q-mu-g-ky-ru
“dry” coe eclogite	g-cpx-ru-coe	coe-mu-g-ky-ru
ab-ep amphibolite	ab-chl-hb-ep	q-mu-g-bi-chl
amphibolite	pl-hb-ilm	q-mu-g-st-bi- q-mu-g-bi-ky/sil
high-grade amphibolite	pl-hb-ilm	q-g-bi-sil-melt
LP granulite	pl-cpx-opx-(hb)	q-kfs-g-crd/opx-(bi)-sil-melt
HP granulite	pl-cpx-g-(hb)	q-kfs-g-opx-ky-(bi)-melt

Table 2. Key mineral assemblages in metabasites and metapelites defining the main metamorphic facies (Manzotti and Ballèvre 2024).

ACFM: metapelites across the Alps

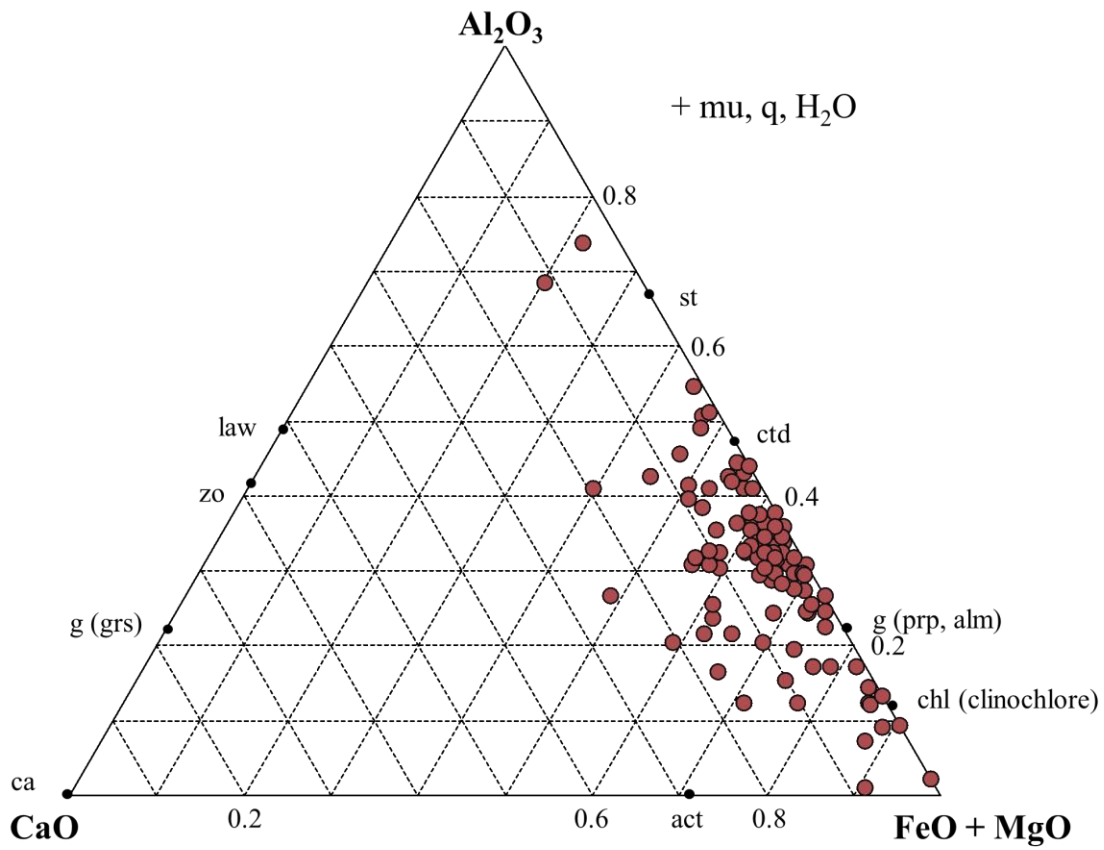


Figure 35. ACFM diagram showing all samples ($n=105$) uncategorized.

ACFM: metapelites in the Western vs. Central vs. Eastern Alps

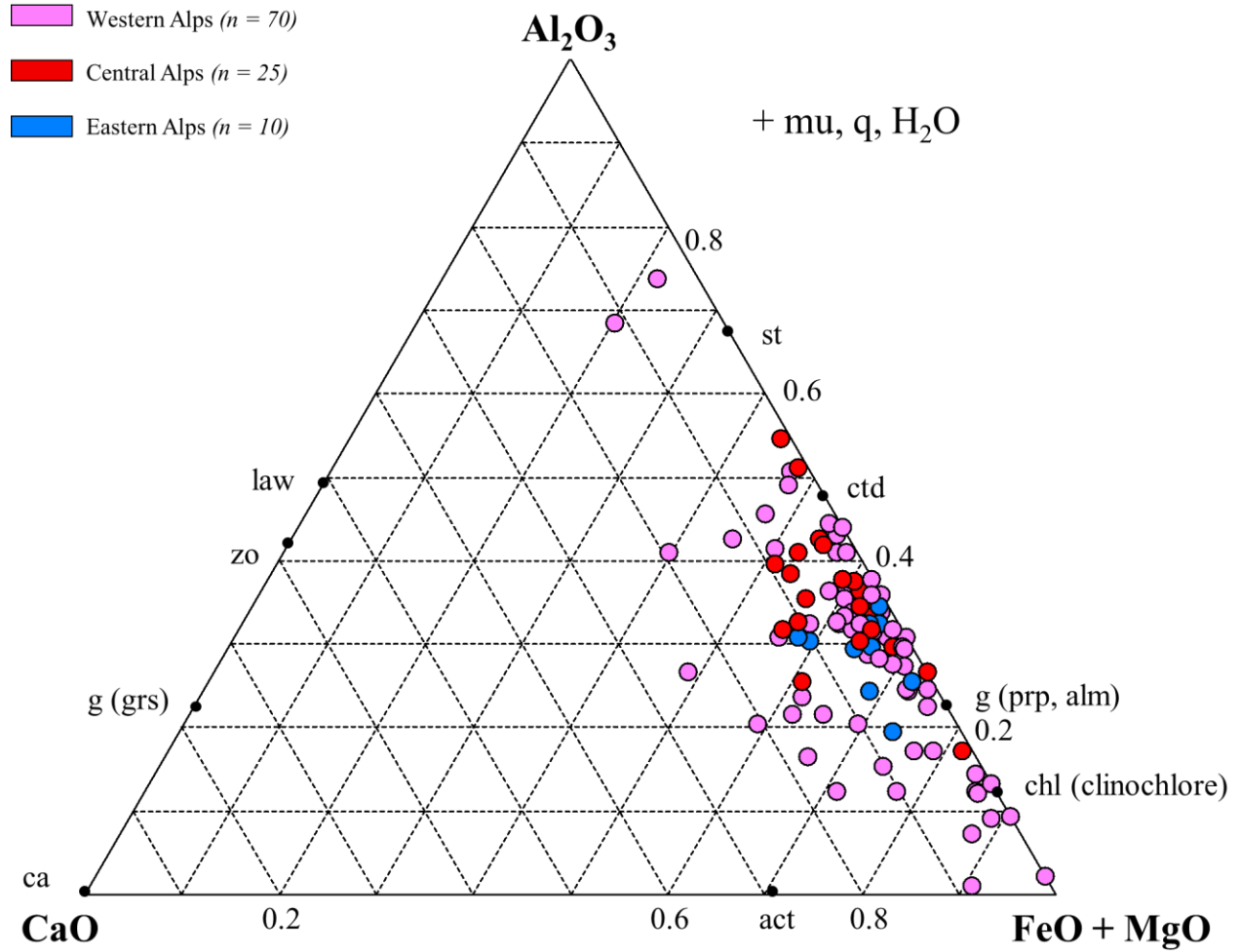


Figure 36. ACFM diagram showing all samples ($n=105$) plotted as a function of their geographical position (Western, Central and Eastern Alps).